# MHD FLOW VISUALIZATION OF MAGNETOPAUSE BOUNDARY REGION VORTICES OBSERVED DURING HIGH SPEED STREAMS

**Yaireska M. Collado Vega**

A thesis submitted in partial fulfillment of the requirements for the degree of

MASTER OF SCIENCE
IN
PHYSICS

UNIVERSITY OF PUERTO RICO
MAYAGÜEZ CAMPUS

2007

Approved by:

| | |
|---|---|
| Pablo J. Marrero Soto, Ph.D.<br>President, Graduate Committe | Date |
| Mark J. L. Chang, Ph.D.<br>Member, Graduate Committe | Date |
| Ramona L. Kessel, Ph.D.<br>Member, Graduate Committe | Date |
| José Rosado, Ph.D.<br>Representative, Graduate Studies | Date |
| Hector Jiménez, Ph.D.<br>Physics Department Chairperson | Date |

# Abstract

We present statistics for a total of 304 vortices found near the ecliptic plane on the magnetopause flanks, using simulated Magnetohydrodynamic (MHD) data driven by real solar wind conditions. The study concentrates on nine hours, from March 29 2000 UT to March 30 0500 UT, during the onset of a high speed stream that exists from March 29 to April 5, 2002. Magnetopause crossings seen by the Geotail spacecraft for the nine hours time interval were also analyzed and compared with the MHD simulation to validate our results. Vortices were classified by solar wind input provided by the Wind satellite located 60-80 $R_E$ upstream from Earth. 273 of the vortices were generated under northward Interplanetary Magnetic Field (IMF) and 31 were generated under southward IMF. The vortices generated under northward IMF were more prevalent on the dawnside than on the duskside, and were substantially less ordered on the dawnside than on the duskside. Most of the vortices were large in scale, up to 10 $R_E$, and with a rotation axis closely aligned with the $Z_{SM}$ direction. They rotated preferentially clockwise on the dawnside, and counter-clockwise on the duskside. Those generated under southward IMF were less ordered, fewer in number, and also smaller in diameter. Significant vortex activity occurred on the nightside region of the magnetosphere for these southward cases in contrast to the northward IMF cases on which most of the activity was on the magnetopause flanks. The IMF is primarily northward for our time interval and the development of these vortices with their rotation preference depending on their local time position suggest that a Kelvin-Helmholtz (KH) instability is likely present.

# Resumen

Presentamos estadísticas de un total de 304 vórtices encontrados en los bordes de la magnetopausa cerca del plano eclíptico, utilizando datos de una simulación Magnetohidrodinámica derivada de condiciones reales del viento solar. Este estudio se concentra en nueve horas, desde el 29 de marzo 2000 TU hasta el 30 de marzo 0500 TU, en donde se encuentra el comienzo de un flujo de viento solar a alta velocidad que dura desde el 29 de marzo hasta el 5 de abril del año 2002. Cruces de la magnetopause captados por el satélite Geotail entre estas nueve horas de estudio fueron tambien estudiados y comparados con los datos de la simlación MHD para validar nuestros resultados. Los vórtices fueron clasificados utilizando condiciones del viento solar obtenidos del satélite Wind el cual se encuentra a 60-80 $R_E$ de la tierra. 273 de los vórtices fueron generados bajo condiciones del IMF hacia el norte y 31 de los vórtices fueron generados bajo condiciones del IMF hacia el sur. Los vórtices generados bajo las condiciones hacia el norte del IMF ocurrían en mayor número en el área del amanecer que en el área del anochecer, siendo sustancialmente menos ordenados en el área del amanecer que en el área del atardecer. La mayoría de los vórtices eran grandes a escala, hasta 10 $R_T$, y con el eje de rotación alineado a la dirección del eje de $Z_{SM}$. Preferiblemente estos rotaban a favor de las manecillas del reloj en el área del amanecer, y en contra de las manecillas del reloj en el área del atardecer. Aquellos vórtices generados bajo condiciones del IMF hacia el sur eran menos organizados, menos en número, y también más pequeos en tamaño. Una significante cantidad de vórtices ocurrieron el la parte nocturna de la magnetosfera para estos casos del IMF hacia el sur en contraste con aquellos que ocurrieron durante el IMF hacia el norte

en donde la actividad era concentrada hacia los bordes de la magnetopausa. El Campo Magnético Interplanetario (IMF) es en su mayoría en dirección hacia el norte para nuestro intervalo de tiempo en estudio y el desarrollo de estos vórtices con su preferencia en rotación dependiendo en su localidad, claramente sugieren la presencia de una inestabilidad tipo Kelvin-Helmholtz para nuestro intervalo de tiempo en estudio.

# Dedicatory

*First of all, I would like to dedicate my work to God. Without His help I wouldn't be where I stand right now. Second, my family; they gave me the strength and the hope to stay and fight for what I believed. They are my fort and my soul. This work is also dedicated to the memory of many family members I've lost throught these years of college, specially my dearest aunt Cruz Maria Collado Torres (Titi Cuqui).*

# Acknowledgements

I would like to aknowledge my advisor from NASA/GSFC Dr. Ramona Kessel. Thank you for all your support. Also, my research group: Dr. Xi Shao, Dr. Virginia Kalb and Ryan Boller. Everyone from the old Space Physics Data Facility at GSFC (code 632) now the Heliospheric Physics Laboratory (code 672), specially my supervisor Dr. Robert McGuire. Dr. Timothy E. Eastman of QSS Group, Inc. for his assistance in evaluating this work. SSCWeb for their orbit and trajectory services, and CDAWeb for their satellite data services (http://spdf.gsfc.nasa.gov).

Also, thanks to my dearest friends that fought with me at the same time throught my bachellors in Physics; Carlos, Teddy, Evelyn, Emily, Alexandra, Freddie, Yaitza, Carlos Santana, and our youngest Luis Balbino. Also my friends from the outside world: Suzanne, Daphne, Vanessa, Hector Luis, Jeyra, Zuleika, and Erin. They are the kind of friends that support you no matter what. Thank you Joel for your love, kindness and support. Last, but not least, my professors of UPRM: Dr. José R. López, Dr. Pablo Marrero, Dr. Mark Chang, Dr. Erick Roura, and Dr. Carlos Pabón, which gave me the hard work that I needed to become the physicist that I am right now. Thank You.

# List of Figures

# List of Abbreviations

CPI - Comprehensive Plasma Instrument

GSFC - Goddard Space Flight Center

IDL - Interactive Data Language

IMF - Interplanetary Magnetic Field

KH - Kelvin-Helmholtz

LFM - Lyon-Fedder-Mobarry

MagCon - Magnetospheric Constellation

MFI - Magnetic Field Instrument

MGF - Magnetic Field Measurement

MHD - Magnetohydrodynamic

MMS - Magnetospheric Multi-Scale

$R_E$ - Earth Radii

SM - Solar Magnetic Coordinates

SWE - Solar Wind Experiment

UT - Universal Time

# Contents

# Chapter 1

# Introduction

The Earth's magnetosphere is the geomagnetic cavity that protects the Earth against the high energy particles from the Sun. The velocity and pressure from this stream of particles, called the solar wind, causes the Earth's magnetic field to squash in one side and stretch at the other forming a big tail, called the magnetotail. Figure 1.1 shows a simple 2D sketch of the magnetosphere structure that has been inferred by spacecrafts observations. Three of the main magnetosphere's features are the bow shock, the magnetosheath and the magnetopause. The bow shock is the front boundary that causes the solar wind to be slowed and deflected. The inner boundary of the magnetosphere is called the magnetopause, and the region between the bowshock and the magnetopause is called the magnetosheath.

The solar wind provides source energy for many magnetospheric processes. One such process is that of surface waves driven near the outer magnetospheric boundary and magnetopause by the kinetic energy of bulk plasma motion. Surface waves can be subject to instabilities. One of the most familiar is the Kelvin-Helmholtz (KH) instability (see Appendix 1), which arises when waves are excited at boundaries with velocity shears. The non-linear stage of this instability can create vortex events that can lead to the interaction between the fluids of the two sides of the boundary (see Figure 1.2).

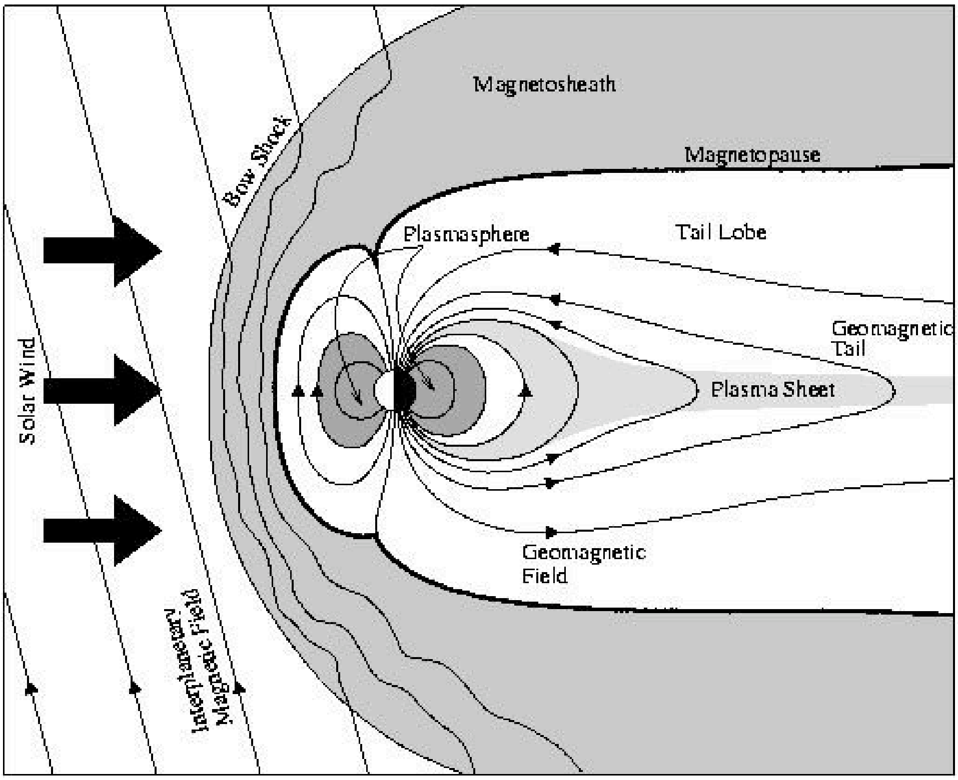


Figure 1.1: Simple magnetosphere structure as has been inferred by spacecraft observations over the years. Figure from www.tp.umu.se/ forskning/space/.

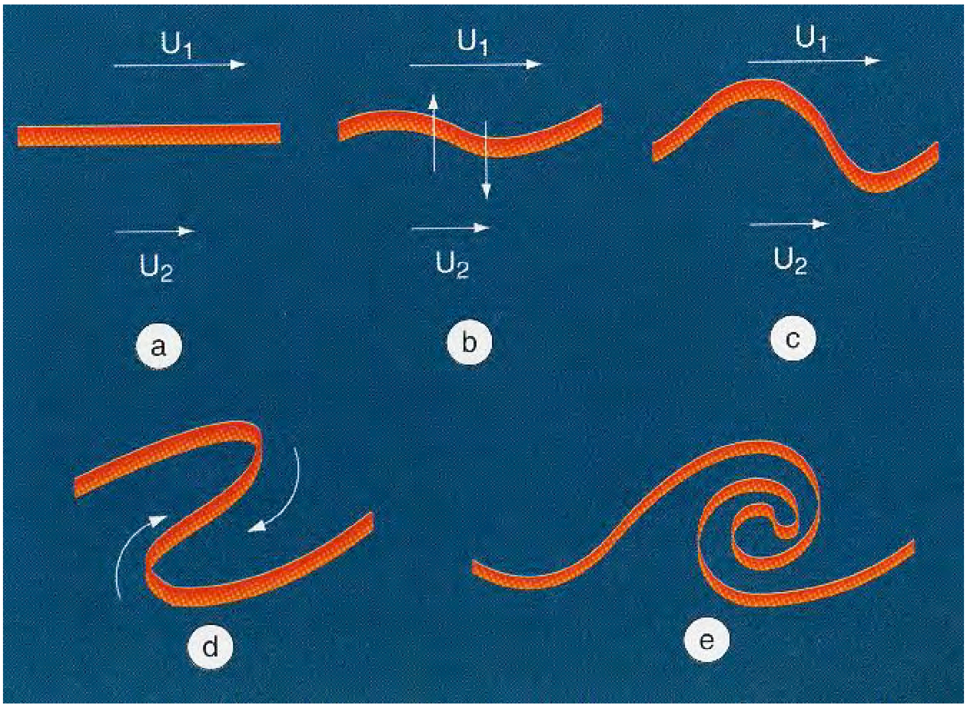


Figure 1.2: Two horizontal streams with different velocities, *U1* and *U2*, and different densities. The upper stream is faster than the lower making the shear unstable until a rolled up vortex is formed (a-e). Figure from http://www.enseeiht.fr/hmf/travaux/CD0001/travaux/optmfn/hi/01pa/hyb72/kh.

When looking at the magnetosphere, the processes that occur at the magnetopause are the ones responsible for determining how much energy the magnetosphere receives from the solar wind. When the solar wind reaches the Earth, the velocity shear between the magnetosheath and the magnetospheric plasma can create large rolled up vortex events that can be associated with the transport of the solar wind plasma into the magnetosphere. These kind of KH vortices have been closely related to the direction of the north component of the interplanetary magnetic field (IMF) [Chen et al., 1993; Chen and Kivelson, 1993; Otto and Fairfield, 2000; Takagi et al., 2006; Hasegawa et al. 2006]. The study of these kinds of processes is not only of interest for scientific research, but also for its impact on human activity via geomagnetic disturbances.

Scientific modeling is very important for the study of the Earth's magnetosphere, considering that observational data is very difficult to obtain because of the few probes available. Nowadays, a mission called Cluster has four satellites in tetrahedral formation, and is the only satellite capable of studying small-scale structures of the magnetosphere in three dimensions. New missions like the Magnetospheric Multi-Scale (MMS) and the Magnetospheric Constellation (MagCon) will use similar configurations and will enhance the spatial component of observation. New modeling and visualization tools are necessary to adequately treat the data from these new multiple spacecraft missions. This will help us improve our understanding of the complex particles interactions and disturbances in our geospace environment caused by the solar wind. The creation of better visualization tools will not only maximize our understanding of processes taking place around our Sun-Earth environment, but will also enhance our scientific input and output for new and future missions.

Since 2004, NASA Goddard Space Flight Center (GSFC) funding has been directed to the development of a cross-platform visualization tool written in Interactive Data Language (IDL) called "MHD Explorer". This tool reads large amounts of data from MHD simulations and has the capability to show 2D and 3D overviews of the plasma flow global topology in user-selected magnetosphere regions. It can also be used to create animations that will clearly show the evolution of complex interactions of geospace processes, like rolled up vortices in the magnetopause.

In this study, an MHD simulation driven by real solar wind conditions was visualized in the magnetospheric equatorial plane and compared with satellite data near the magnetopause boundary. To the best of our knowledge the visualization of MHD data presented here using *MHD Explorer* is the first to show the evolution of flow vortices. We focused on Wind data for the time interval of March 29 2000 UT to March 30 0500 UT, 2002 that was at the onset of a high speed stream, that lasted for eight days with predominantly northward IMF. The magnetopause was characterized by substantial vortex development with a preference in rotation direction. This preference in rotation has also been associated with the KH process [Hones et al., 1978; Hughes, 1994]. However, there were times when the IMF turned southward, and some vortices were also found in the magnetosphere for these times. Altogether we examined 304 3D vortices that we characterized by input solar wind conditions.

The presentation of this work is as follows: chapter 2 presents some background literature of MHD modeling. Chapter 3 gives a simple description of the data and methods used for this study. In chapter 4, we describe the vortices found in the magnetopause region during this time interval for northward and southward IMF. Chapter 5 compares the MHD simulation with boundary crossings observed from the Geotail spacecraft. Discussion and closing remarks constitute chapter 6.

# Chapter 2

# Literature Review

Surface waves can be driven near the outer magnetospheric boundary and the magnetopause by the kinetic energy of bulk plasma motion. The Kelvin-Helmholtz (KH) instability arises when MHD waves are excited at the magnetopause when the magnetosheath plasma flows past the magnetosphere providing a velocity shear [Ogilvie and Fitzenreiter, 1989]. If the velocity shear reaches a critical speed that overcomes the magnetic tension resisting any force trying to stretch the boundary, wave growth may occur [Miura, 1995; Kivelson and Chen, 1995]. The growth rate of this waves depend on local properties of the plasma and the thickness of the boundary layer.

The theory of Hasegawa [1975] indicates that equatorial regions of the magnetopause are likely to be most unstable when the magnetic field component is perpendicular to the flow velocity. Chen, et al. [1993] studied the significant role that the magnetosheath magnetic field played not only on the flow velocity but also on the shape of the magnetopause. In their study they showed evidence of high speed flows ($>$Vsw) in the low-latitude magnetosheath during northward IMF and found surface waves of very nonsinusoidal form of $\sim$ 5 min period that they attributed as a consequence of the non-linear stage Kelvin-Helmholtz instability. Later, in that same year, Chen and Kivelson showed results for 1 hour interval that were at variance with numerical models of nonlinearly growing KH waves which have steepened slopes at the downstream edges. They propose that the anomalous form of the waves arose because of dominant and positive $B_Z$ component at the magnetosheath.

Many theoretical models and simulations over the years have been developed to characterize the magnetic field and the flow velocity [Miura, 1984, 1987, 1992; Wei et al., 1990; Fujimoto and Terasawa, 1994; Otto and Fairfield, 2000]. Miura [1984] made a model of magnetospheric boundaries at high latitudes with the flow velocity parallel to the magnetic field ($\mathbf{v}_0||\mathbf{B}_0$), and dayside low latitudes with a substantial transverse component ($\mathbf{v}_0 \perp \mathbf{B}_0$). Miura's model was intended to study the anomalous magnetospheric viscosity caused by the KH instability.

Later, Miura [1987] performed a two dimensional MHD simulation of the magnetospheric boundary including gradients of plasma and magnetic field normal to the dayside low-latitude magnetospheric boundary. Miura observed that for the right set of parameters at the dayside magnetospheric boundary the anomalous viscosity obtained is the right magnitude to drive magnetospheric convection in the Earth's magnetosphere. Wei et al., [1990] studied a two-dimensional incompressible hydrodynamic model driving plasma into the boundary layer by a diffusive flux along the magnetopause. They observed vortex motions associated with the KH instability that convect tailward by the flow velocity and grow in size.

Using his 2D study, Miura [1992] showed that the KH instability can also develop in the far tail flanks of the magnetosphere. Fujimoto and Terasawa, [1994] conducted a hybrid code simulation of MHD-scale tranverse KH instability in a uniform plasma to study the ion mixing process within a KH vortex. Otto and Fairfield, [2000] used a numerical method, which showed the development and growth of vortices during a time that Geotail observed crossings at the equatorial magnetotail boundary with parallel northward fields between the Earth's magnetic field and the IMF. Later, Takagi et al. [2006] performed a three dimensional MHD simulation that showed highly tail flanks KH rolled up vortices when the magnetosheath field is norhtward and the plasma sheet is thicker than a few $R_E$.

Dungey [1961] proposed that large scale magnetic reconnection was the most important process for particles crossing at the magnetopause. However, Otto and Fairfield [2000] results showed that localized magnetic reconnection occurs within the magnetic field twisted by the KH vortex motion, thus making possible mass transport to the magnetosphere. Takagi et al. [2006] also suggested that the KH vortices played a significant role in plasma transport across the boundary under northward IMF, which was supported by Hasegawa et al. [2006] identifying rolled up vortices with in situ measurements and detecting magnetosheath-like ions at the magnetospheric side of the boundary in all the cases. These studies demonstrate that KH instability can be a significant contributor to the transport of energy, momentum, and also mass into the magnetosphere.

# Chapter 3

# Data and Methodology

## 3.1 Data

For this study we used data from the Wind and Geotail satellites for the time interval of March 28 to April 5, 2002. Wind was located 60-80 $R_E$ upstream and Geotail was skimming the magnetopause at a radial distance of 25-28 $R_E$. A 3D orbit plot is shown in Figure 3.1 for better visualization on the satellites location. We used the Magnetic Field Investigation (MFI) [Lepping et al., 1995] and Solar Wind Experiment (SWE) [Ogilvie et al., 1995] instruments from the Wind satellite, and the Magnetic Fields Measurement (MGF) [Kokubun et al., 1994] and Comprehensive Plasma (CPI) [Frank et al., 1992] instruments from Geotail.

The interval of March 28 to April 5 is marked by a high speed solar wind stream, as shown by Wind data in Figure 3.2 top panel. Its initial velocity increase takes place during the last four hours of March 29, and then continues increasing for two days. After the second day, it begins to decrease to a nominal value of 400 km/s, which is a typical solar wind speed. The next two panels show a region with an increase in dynamic pressure and magnetic field magnitude. This increase occurs at the leading edge of the high speed solar wind stream and lasts for 10 hours between the

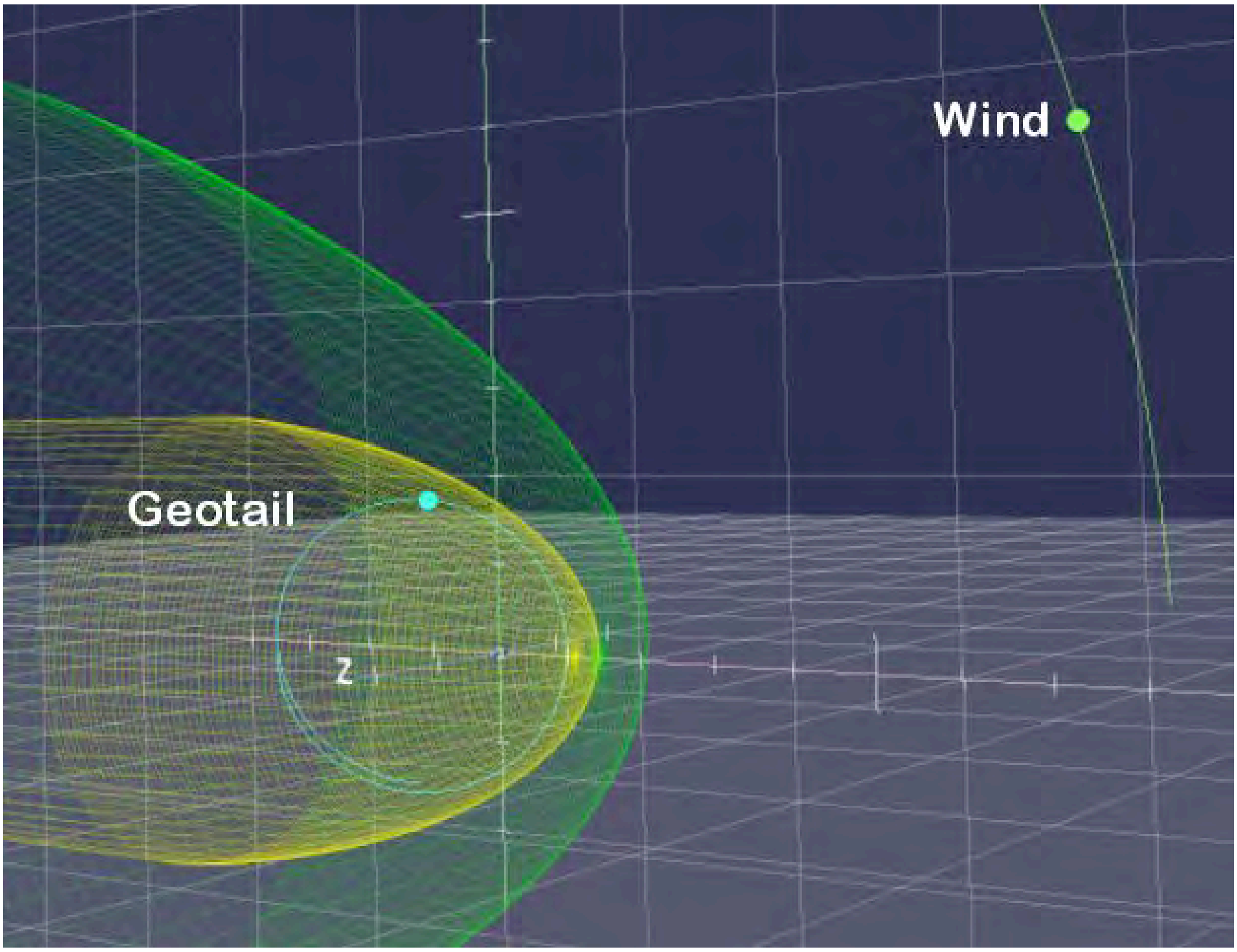


Figure 3.1: A 3D orbit plot of the two satellites location within the time interval of March 28 to April 5, 2002. Geotail is skimming the magnetopause and Wind is located 60-80 RE upstream.

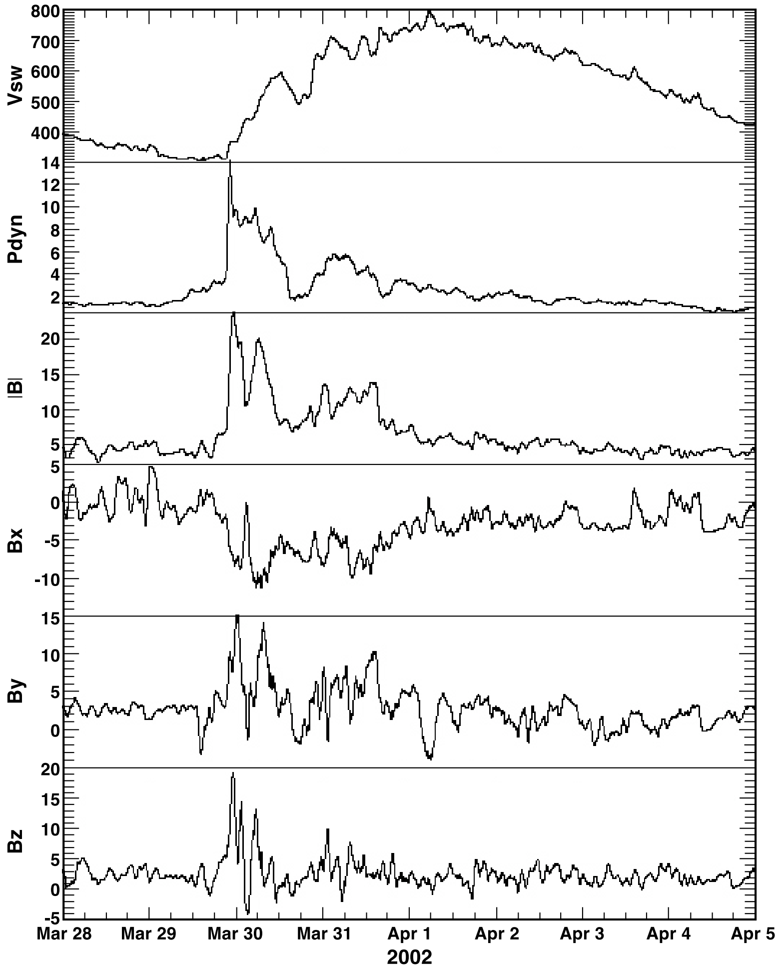


Figure 3.2: The top panel shows average values for the high speed solar wind stream from March 28 to April 5, 2002. The next two panels show increases in dynamic pressure and magnetic field magnitude, and the last three panels show the *Bx*, *By*, and *Bz* components of the magnetic field. The *Bz* component is predominantly positive for the whole time interval.

days of March 29 and March 30. There is a second increase after noon on March 30 but of a smaller magnitude. Between the first hours of April 1, the dynamic pressure and magnetic field magnitude show nominal values of 1 nPa and 5 nT, respectively. The last three panels show the $Bx$, $By$ and $Bz$ magnetic field components for this time interval. The variations in the transverse component are small, and the positive $Bz$ component show that for most of the time interval we have a strong northward IMF.

## 3.2 Simulation

The Lyon-Fedder-Mobbary (LFM) global MHD model [Fedder et al., 1995] is a comprehensive model composed of a number of interacting modules specifically designed to provide dynamic images of geospace and having the capability to be tested against "ground truth" - quantities measured in space or on the ground. It is a continuously evolving model improving its various modules following comparisons with the assimilated data. The core module is a three dimensional MHD code that solves the ideal MHD equations in a conservative form. These equations are discretized and solved on a cylindrical staggered mesh, typically 60 $R_E$ in radius and 330 $R_E$ long, containing the solar wind and the magnetosphere. A spider web type computational grid places maximal resolution on physically critical locations such as the discontinuities, plasma sheet, inner magnetosphere and dayside magnetopause. The code uses diffuse solar wind matching conditions along the outer edges of the computational domain. This permits time dependent solar wind parameters as input conditions. A simple supersonic outflow condition is used in the outer anti-solar boundary. The code has the capability to be initiated at the upstream boundary with data taken from upstream satellites. The inner boundary condition is located on a geocentric sphere of radius 2-3 $R_E$, where the magnetospheric solution is matched to the solution of the ionospheric module.

The second module represents the ionosphere. It solves the two-dimensional height integrated electrostatic potential equation driven by the field-aligned currents within the magnetosphere,

$$\nabla_\perp \bullet \mathbf{\Sigma} \bullet \nabla_\perp \mathbf{\Phi} = \mathbf{J} \bullet \hat{\mathrm{b}} \tag{3.1}$$

where $\mathbf{\Phi}$ is the ionospheric potential, and $\mathbf{\Sigma}$ the anisotropic conductivity tensor. The term $\mathbf{J} \bullet \hat{\mathrm{b}}$ where $\hat{\mathrm{b}}$ is the unit vector along the magnetic field direction, is a critical term since it represents the coupling between the ionosphere and magnetosphere. This parallel current is mapped into the ionosphere along unperturbed dipole magnetic field lines. The height-integrated current continuity equation yields the perpendicular current density (both Hall and Pedersen) in the ionosphere. An important input to the code is the height integrated conductivity tensor $\mathbf{\Sigma}$ that has a component computed on the basis of the solar EUV flux and a component based on the auroral precipitation [Fedder et al., 1995]. The conductance tensor has both Pedersen and Hall components. The LFM code has been benchmarked in accomplishing key global magnetospheric science objectives [Papadopoulos et al., 1999; Papadopoulos, 2000]. In addition to the event studies, the LFM model was used to benchmark a number of northward IMF cases [Guzdar et al., 2001; Shao et al., 2001] as well as to simulate $>$10 intervals totaling 550 hours from data compiled by Bargatze et al. [1985]. Namely, the LFM simulations were driven by the solar wind conditions observed during the intervals of the Bargatze data set. A data set similar to that of Bargatze was constructed from simulation. Both sets were treated as input-output systems with the solar wind input function VBz and the AL auroral activity index as output. In this way, the LFM model was statistically benchmarked with observations [Shao et al., 2003].

In this study, the simulation was performed in the Solar Magnetic (SM) coordinate system allowing for the tilt of the Earth's magnetic dipole relative to the solar wind flow direction to be included. On this coordinates system the $Z$-axis is chosen parallel to the north magnetic pole and the $Y$-axis perpendicular to the Earth-Sun line towards dusk. Outflow conditions are imposed on the downstream boundary. Elsewhere, external boundary conditions were specified using ACE solar wind data propagated appropriately to the front and cylindrical sides of the grid. The propagation of the ACE solar wind data to the front side of the grid in the LFM model is described in detail in Wiltberger et al. [2000]. The spider web type computational grid places maximal resolution approximately 0.2 RE on locations such as the discontinuities, inner magnetosphere and dayside magnetopause.

## 3.3 Visualization

A display tool in Interactive Data Language (IDL) called "MHD Explorer" was used to examine the development of vortices on the magnetopause flanks. This tool reads large amounts of data from the Lyon-Fedder-Mobarry (LMF) global MHD code [Fedder et al., 1995; Lyon et al., 2004]. The global MHD simulation results (one-minute resolution plasma and magnetic field data files) are used with our visualization tool. Reading plasma data files from the LFM code, the MHD Explorer tool can be used to display both 2D and 3D overviews, giving an example of the magnetospheric flows in SM *(x, y, z)* coordinates. For the 3D overview the tool performs an IDL "particle trace" procedure which uniformly releases massless particles into a specified 3D volume and then traces them through a vector field built from the grid flow velocities.

Using this visualization tool, we searched MHD simulation data for vortices within nine hours of the time interval shown in Figure 3.2. The time interval corresponds to March 29 2000 UT to March 30 0500 UT. This is the time that the high speed stream begins with the increase also in the dynamic pressure and magnetic field magnitude. Vortices near the magnetopause were examined, parameterized, and categorized in detail for these nine hours. Time shifted values from the Wind satellite were used to parameterize the vortices with solar wind values. The parameters were the solar wind speed, density, dynamic pressure, magnetic field magnitude, and the $Z$ component of the magnetic field vector. Characterization and details of the vortices will be discussed in the next section.

# Chapter 4

# Vortex description using MHD simulations

The visualization tool uses 1 minute plasma data files from the MHD simulation driven by solar wind input from Wind satellite data, and provides 2D and 3D overviews of flow movement. With the 3D window one can select different SM (*x, y, z*) coordinates to search for vortices.

*Movie 1* shows an example of the 2D overview given by our visualization tool. The visualization box spans 15 $R_E$ sunward and -25$R_E$ antisunward in the *x* direction, and +20 to -20 $R_E$ in the *y* direction at the *z*=0 cut plane. The background colormap represents the plasma flow velocity magnitude (speed) in a logarithmic scale shown at the bottom of the box. The speed has a range from approximately 10 km/s (dark green) to 1,000 km/s (red).

The bow shock is represented by the difference in color showing a decrease in the plasma flow speed from 1,000 to around 100 km/s (pink area). The arrows represent the plasma flow direction vectors, which are deflected around the magnetosphere's flanks. The magnetopause boundary is shown by a very thin layer; the plasma flow is deflected around the boundary and the speed changes from 100 km/s to ~60 and 35 km/s (purple and blue layer). The center area, a sphere of radius 5 $R_E$ around [0,0], represents the location of the Earth where no data is recollected.

When running, the movie covers three hours, 2000-2300 UT, of March 29, 2002. We can see the turbulence at noon as the flow deflects around the magnetopause, and focusing on the speed changes around the flanks, many vortices can be spotted. The vortices can be seen by the dark green areas (lower speed) surrounded by light green areas (increasing speed), and with the flow direction vector rotations around their cores. Some of these vortices dissipate, but many are swept tailward along the flanks.

The movie stops for a few seconds on the 2133 UT time frame showing the location of five vortices, four located on the dawnside of the magnetopause and one on the duskside. Then it shows a clear compression of the magnetopause boundary by the solar wind beginning around 2215 UT. This compression increases with time; the number of vortices that developed at the boundary decreases, and their size also decreases.

To follow a vortex development and growth rate, a second movie was created. *Movie 2* shows the 3D structure and movement of a vortex found at 2045 UT of March 29 on the duskside magnetopause. The 2D box on the top left corner shows the location of the vortex and how it moves tailward along the dusk flank. At 2045 UT the flow begins to be unstable as it is clearly seen by the changes in the speed and the flow direction vectors. The vortex takes three minutes to develop, where a clear core is spotted at 2048 UT with a velocity of $\sim$15 km/s. The vortex is rotating counter-clockwise with its rotation axis aligned with the $Z_{SM}$ direction. It grows in size at the same time that it increases its velocity to about 35 km/s at 2055 UT. After this time, the vortex begins to dissipate as can be seen at the end of Movie 2. This movie clearly shows the vortex lifetime of about 7 to 10 minutes.

Using visualization alone with the 3D overview, vortices could be localized and examined in detail taking their exact coordinates in the magnetopause for these nine hours. After all vortices were found and their coordinates taken, we determined corresponding solar wind parameters to help us classify and characterize the conditions at which each vortex developed, and how they evolved through time. As seen in Figure 3.2 northward IMF was observed for most of the nine hours. In the next section we will discuss in more detail the vortices developed under this northward IMF. However, there were cases when the IMF turned southward, and some vortices were found for these conditions although less in number compared to northward IMF cases. The southward cases will be discussed in section 3.2 of this paper.

## 4.1 Vortices with northward IMF

For the northward IMF cases, we categorized the vortices with their corresponding solar wind conditions; we separated the cases into different ranges of dynamic pressure ($nV^2$) and magnetic field magnitude. In total, 273 vortices were found near the ecliptic plane with northward IMF. In Figure 4.1 we show the solar wind parameters for the MHD time interval. Colored regions show where vortices developed as characterized by the dynamic pressure parameter and the magnetic field magnitude. "A" cases constituted 47% of the vortices, which developed for low dynamic pressure (0-5 nPa) and low magnetic field magnitude (5-10 nT). These vortices developed with an approximate time frequency of 1 vortex per minute. Another 41% of the vortices, B, C, D, and E cases, developed at medium dynamic pressure (5-10 nPa) and a range of magnetic field magnitude; for most of the cases $|B| > 15$ nT. Only 12% of vortices, F cases, were found to be present at high dynamic pressure ($>$10 nPa) and also at high magnetic field magnitude ($>$10 nT). For all of these cases, B - F, there was a lower time frequency of development, with 1 vortex every two minutes.

In Figure 4.2 we show 2D overviews of examples for each one of the cases presented in Figure 4.1. The flow velocity (speed) is shown in a logarithmic scale by the background colormap and the arrows show the direction of plasma flow in the equatorial plane. We marked the location where vortices developed for the different times. Focusing on the flow velocity, vortex formations can be seen by dark green areas (lower speed) surrounded by light and darker blue areas (increasing speed) on the magnetopause flanks. The time 2050 UT, which exemplifies an A case, had the highest vortex activity where at least five vortices were found. Following we have vortex developments sampled at 2240 UT, 0525 UT, 0220 UT, 0023 UT, and 2307 UT for the B, C, D, E, and F cases, respectively (see Figure 4.1). For each of these cases fewer vortices developed.

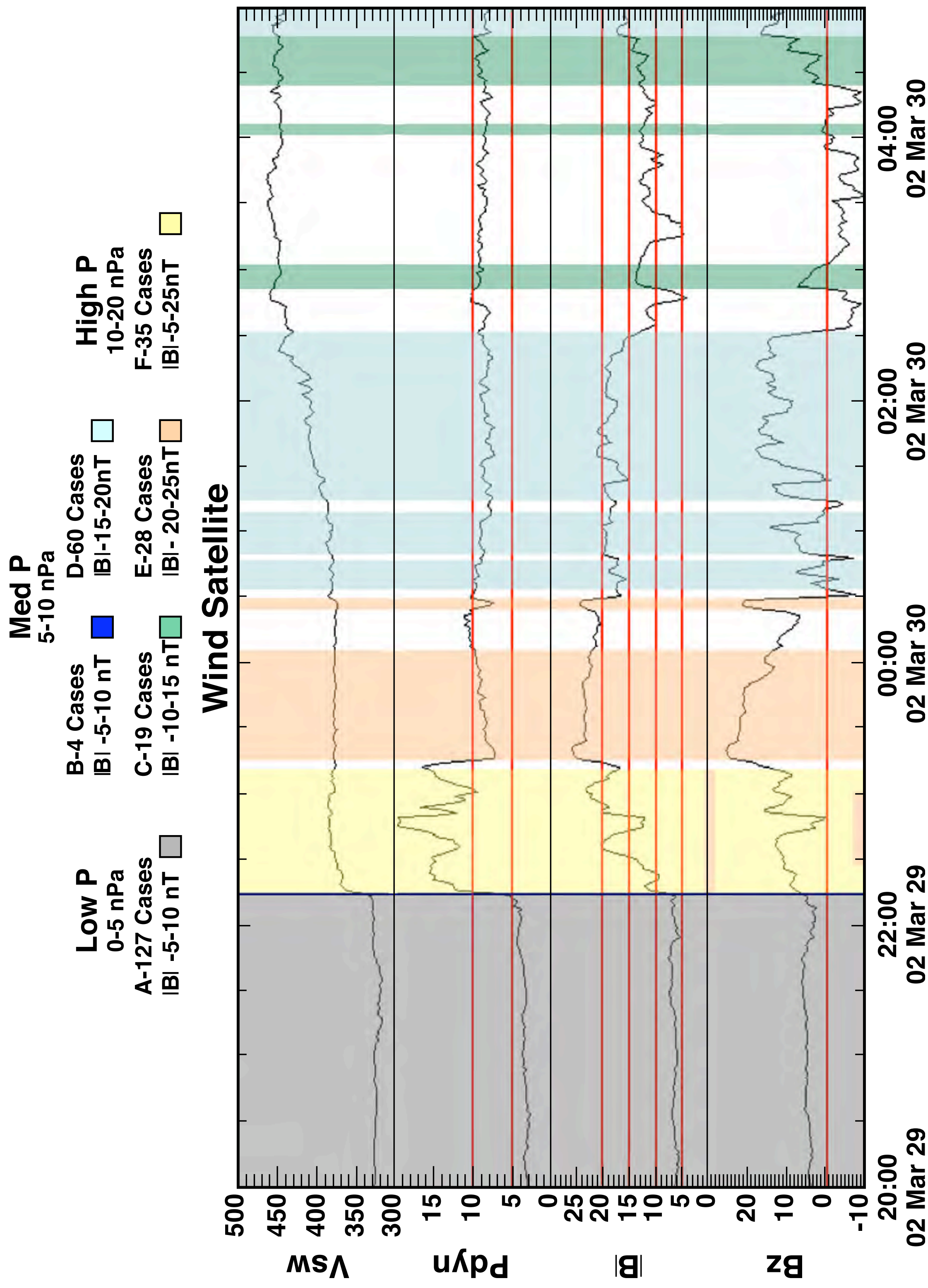


Figure 4.1: Wind solar wind parameters for the MHD time interval. The colored regions show where vortices developed, separated by different value ranges in dynamic pressure and magnetic field magnitude.

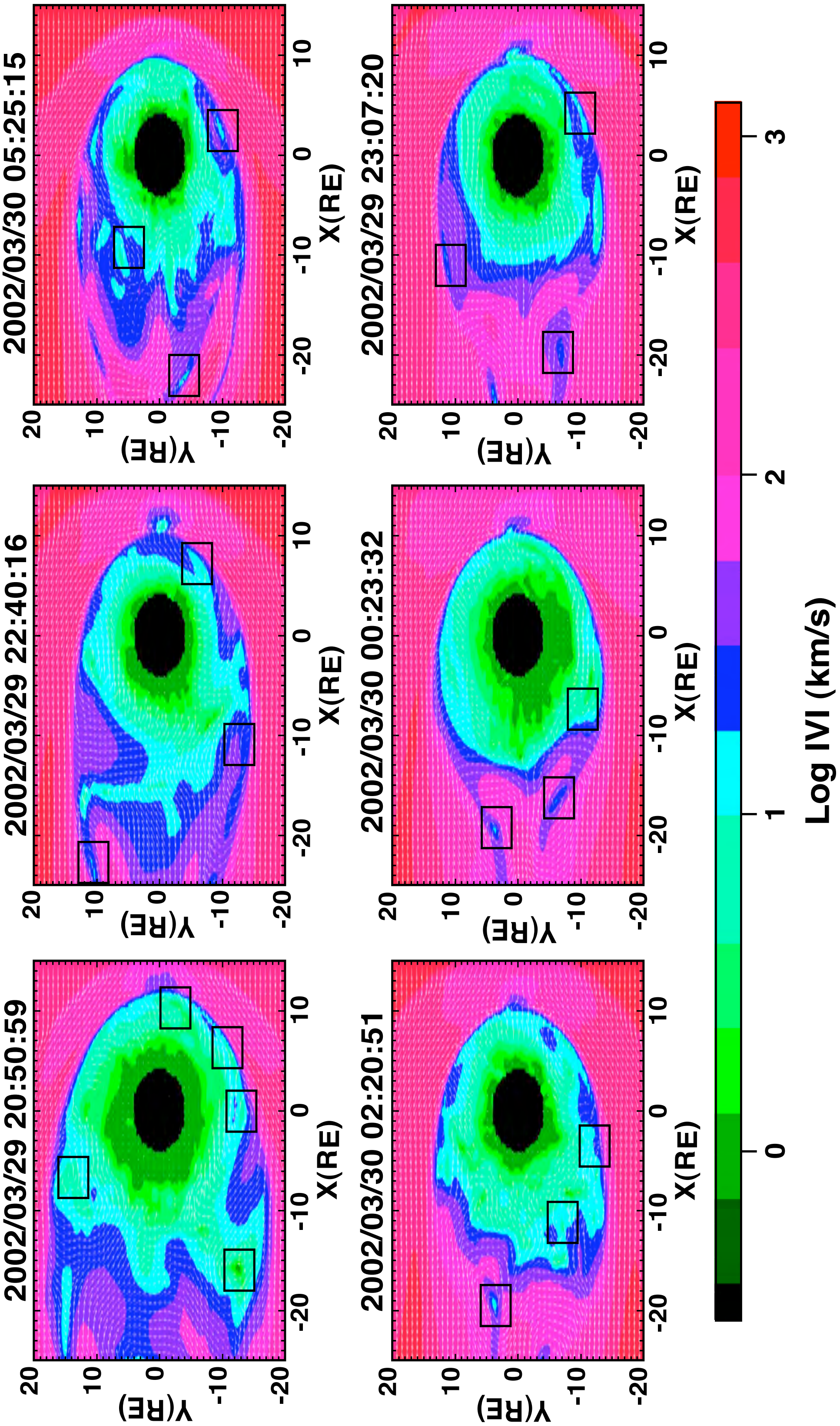


Figure 4.2: 2D overviews of the magnetosphere in the equatorial plane. From left to right; 2050, 2240, 2307 UT (bottom-right) from March 29, and 0525, 0220, 0023, from March 30. Each one correspond to the A, B, C, D, E, and F (left to right) cases, respectively, shown in Figure 4.1. The squares mark where vortices developed for each time. The plasma flow velocity is represented by the background colormap in a logarithmic scale.


Figure 4.3: Percentages of vortices localized on the magnetosphere for 187 vortex cases of northward IMF in two ranges of dynamic pressure and magnetic field magnitude.

Using visualization with the 3D overview we can infer vortex rotation axes, rotation direction (clockwise or counter-clockwise), and scale size. For detailed characterization within the northward IMF cases we concentrated on the A cases of low pressure (<5 nPa) and low magnetic field magnitude (5-10 nT), and the D cases at medium dynamic pressure (5-10 nPa) and higher magnetic field magnitude (15-20 nT). We chose these two parameter regions with the largest number of samples to obtain the most reliable statistics. In Figure 4.3 we characterized the location of vortices; dawn, dusk, nose or tail. Vortices ocurred more often on the dawnside of the magnetosphere than on the duskside. There was also substantial vortex activity near local noon (nose), especially for the 127 "A" cases. For "A" cases, 47% of the vortices developed on the dawnside and 23% were on the duskside. Similarly, for the 60 "D" cases, 48% of the vortices developed on the dawnside and 27% on the duskside.

More than 50% of the vortices propagated in the $x$-$y$ plane having the $z$-axis as their rota-

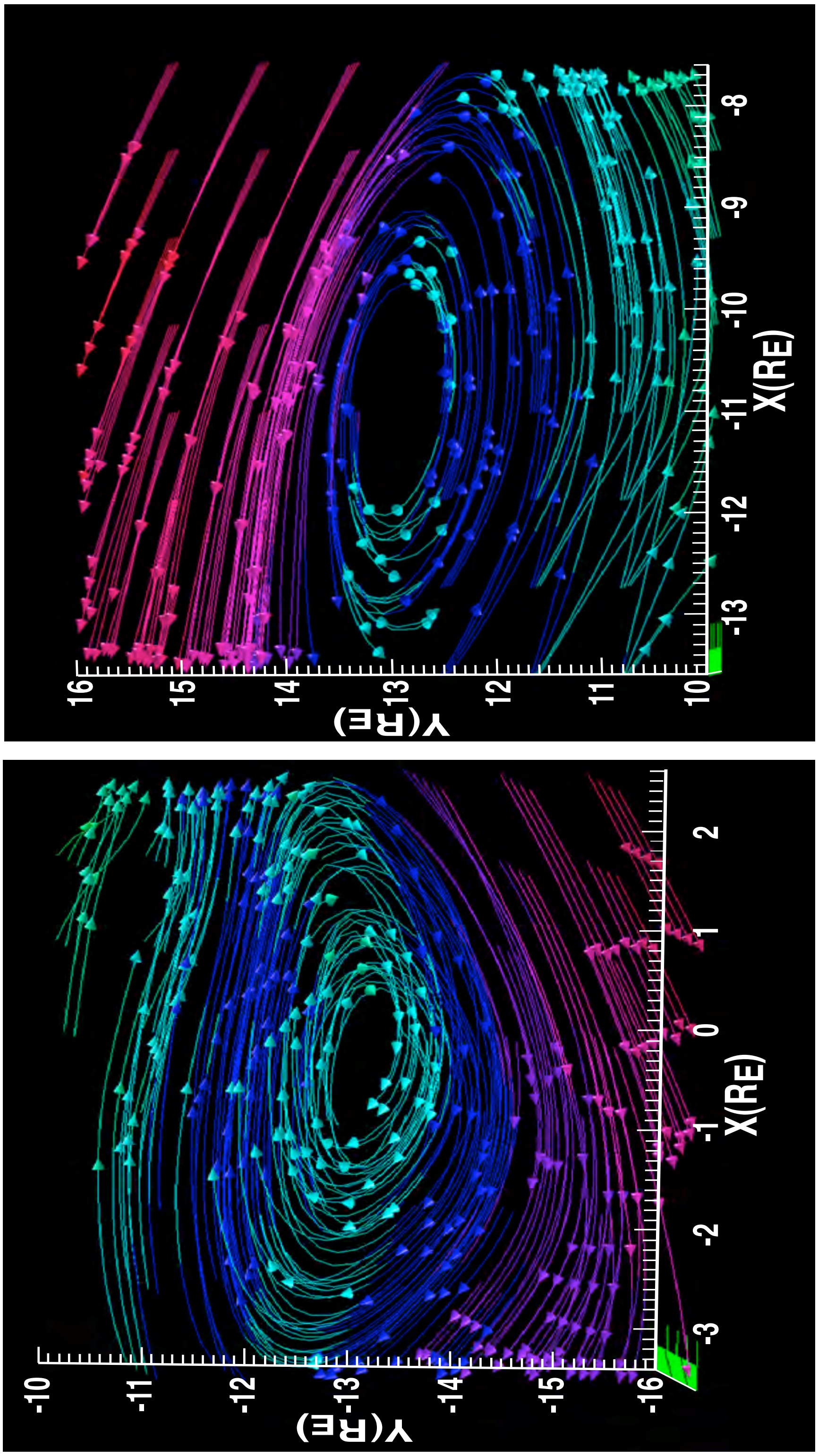


Figure 4.4: A dawn vortex corresponding to March 29 at 2050 UT rotating in the clockwise direction (left). Another vortex corresponding to the duskside of the magnetopause at the time of 2234 UT on the same day rotating counter-clockwise (right).

tion axis for these two cases[1]. They also showed a rotation preference depending on local time position. Dawnside vortices rotated preferentially clockwise, and those at the duskside rotated counter-clockwise. This is shown in Figure 4.4. The vortex that developed on the dawnside (left) is rotating clockwise, while the duskside vortex (right) is rotating counter-clockwise. Both of these vortices have the $z$-axis as their approximate rotation axis. These vortices correspond to the same day, March 29th, but the dawn vortex developed under low dynamic pressure (A case) and the dusk vortex developed under medium dynamic pressure (D case).

Some vortices were large in diameter, up to 10 RE. In Figure 4.5 an example is shown of the large scale of a vortex that developed on the duskside. It also has the $z$-axis as its rotation axis. Dawn vortices were less ordered than those at dusk; for each vortex disordered at the duskside, two were disordered at the dawnside. In the dawn region we also encountered more than one vortex at the same time and at least one of them rotated clockwise. In Figure 4.6 at least five vortices formed on the dawnside, all with different diameters and rotation preferences. In some cases vortices could persist for several minutes while being swept antisunward with the solar wind, which made it more difficult on the flanks to separate original cases from more evolved cases. Most of this type of vortex signature, large in diameter and several in one region, developed under low dynamic pressure conditions. Both of the examples shown correspond to “A” cases in Figure 4.1.

In Figure 4.7 there is also an example of a vortex that developed at local noon (nose) in the outer boundary region corresponding to a D case in Figure 4.1. The vortices that developed at noon were less ordered than vortices that developed at other local times. In Figure 4.7 a large vortex is swept to the duskside while another one is developing on the dawnside. The vortices at the nose did not persist long compared to ones that developed on the flanks. Most frontside vortices disappear in a few minutes, and others are swept antisunward by convection, becoming larger in diameter and changing velocity as they travel along the flanks. In Figure 4.8 a clear progression

[1] The rotation axis alignment can be associated with the IMF direction at the local time position, for all of our A and D cases were predominantly northward.

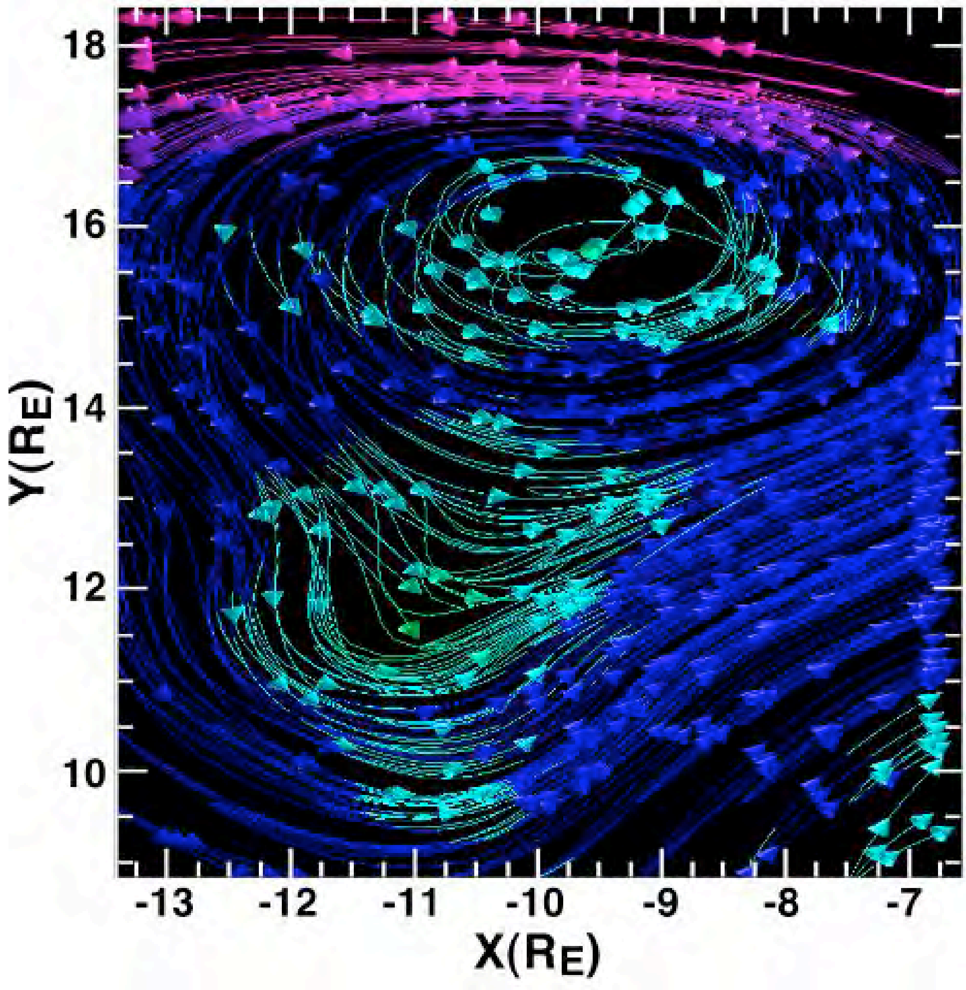


Figure 4.5: A dusk vortex corresponding to March 29 2051 UT with an approximate diameter of 10 RE in scale.

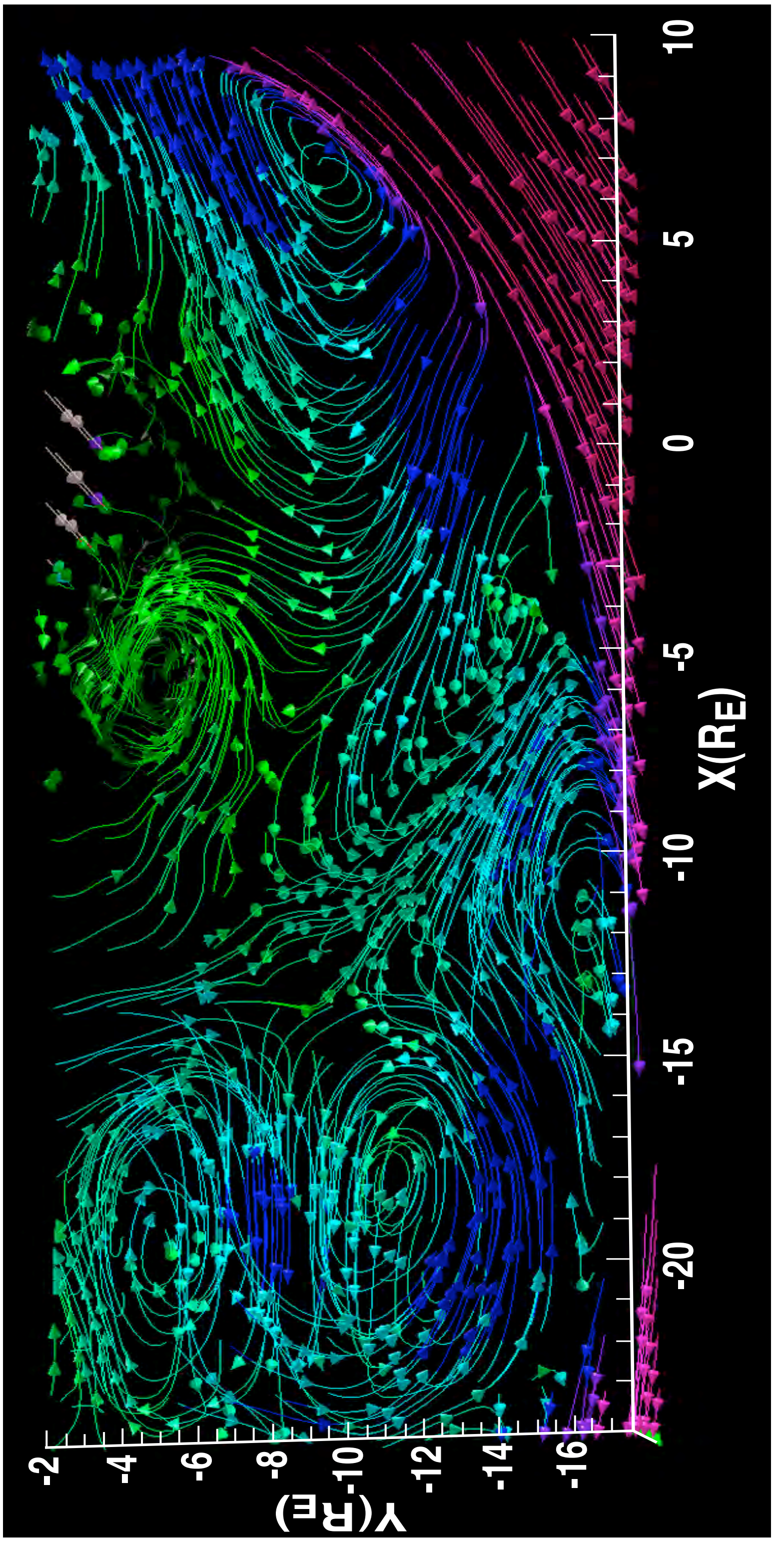


Figure 4.6: Dawnside of the magnetopause in which at least five vortices developed. This overview corresponds to March 29 at 2142 UT.

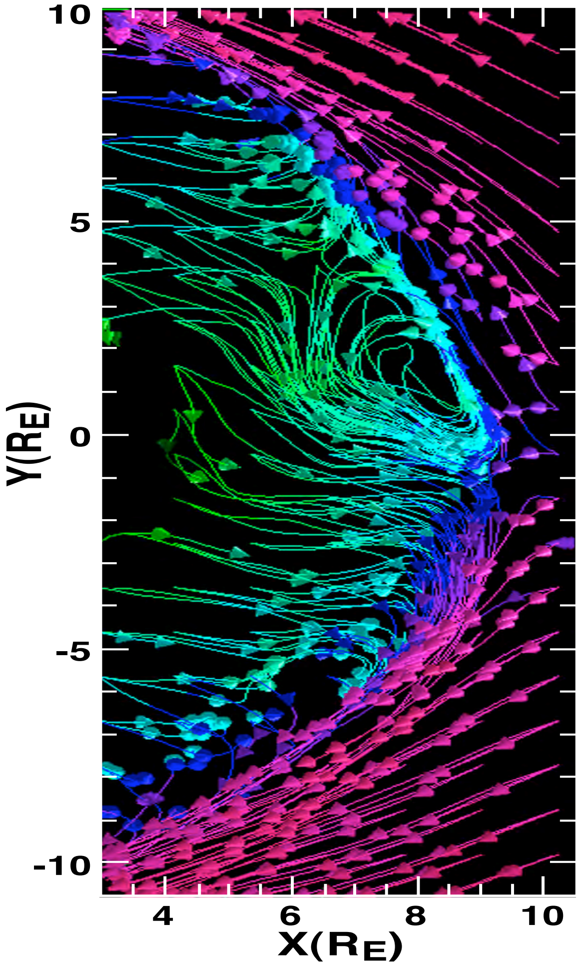


Figure 4.7: One local noon vortex corresponding to March 30 0132 UT is being swept to the duskside while another is being formed on the dawnside.

in vortex development is shown. The vortex corresponds to March 30 (D case) and is traveling antisunward along the dusk flank. Within only four minutes (0246 UT-0249 UT), the vortex core travels approximately 12 $R_E$ down the flank. The velocity of rotation increases significantly along the flank, from 20 km/s to 60 km/s, while its traveling velocity decreases when the vortex becomes fully ordered around 0248 UT.

An interesting fact of the 127 "A" cases at low pressure and low $|B|$ is that they developed before the onset of the high speed stream. For these cases, the solar wind had a velocity average of only 324 km/s. These vortices developed under no particular special conditions for KH vortex

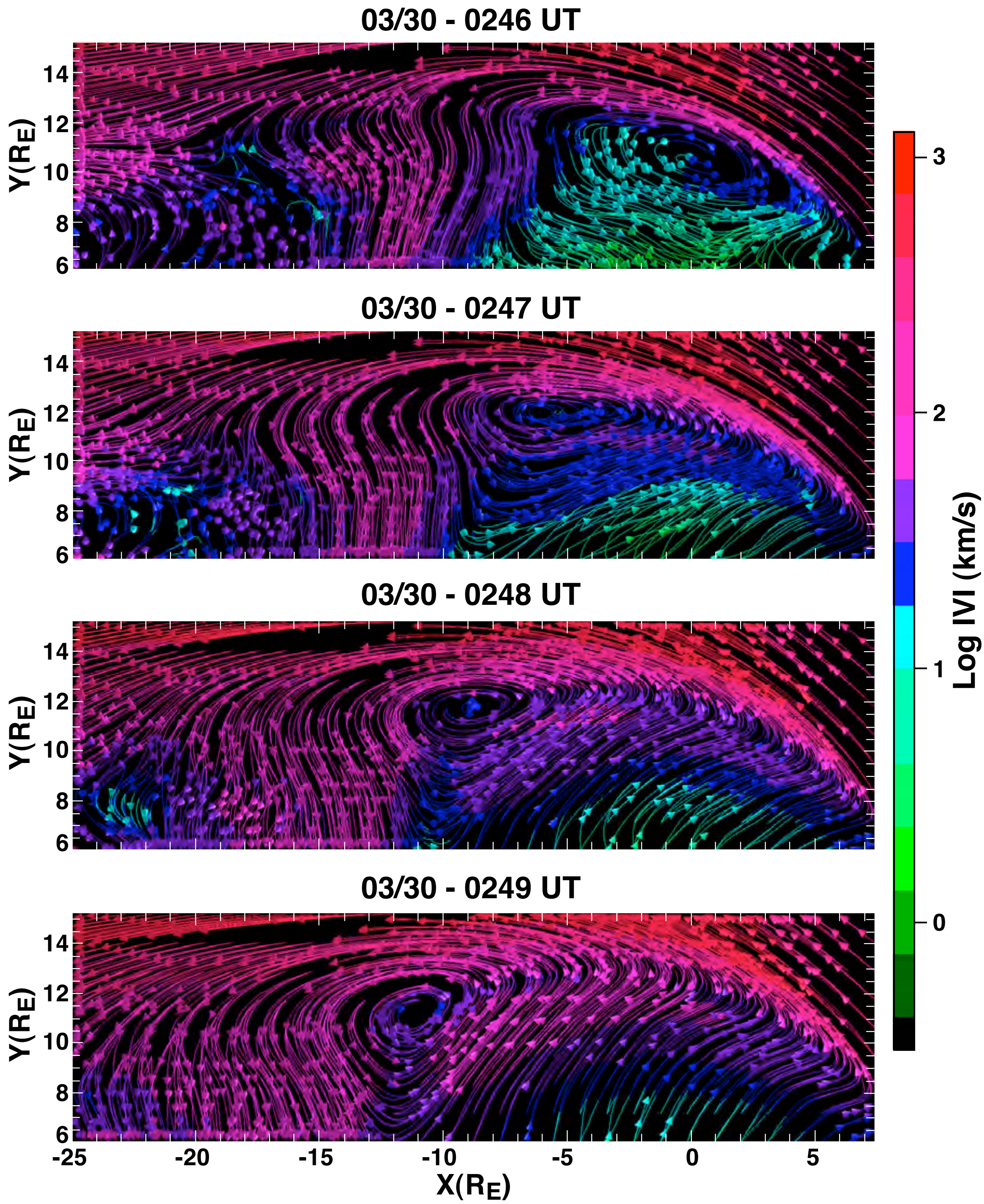


Figure 4.8: Vortex progression of March 30 from 0246 to 0249 UT. The traveling velocity decreases as it rotates antisunward on the dusk flank, but its core velocity increases significantly.

formation. More analysis is being conducted to resolve this question, but that is beyond the scope of this thesis.

## 4.2 Vortices with southward IMF

There were 31 vortices localized near the outer magnetospheric boundary that developed under southward IMF. These cases were also divided between different ranges of magnetic field magnitude, but they only occurred for a pressure range of 5-10 nPa. Conditions for vortices with southward IMF are shown in Figure 4.9 and marked by colored areas. There was no vortex activity out of the dynamic pressure range of 5-10 nPa, but there were different ranges of magnetic field magnitude. Most of the cases were found with higher values of magnetic field as shown in Figure 4.9.

The locations of vortices for southward IMF can be seen in Figure 4.10. For cases with magnetic field magnitude of 5-10 nT, vortices were predominantly found on the dawnside (60%), with 40% in the magnetotail. This reversed as the magnetic field increased its magnitude and most vortices (62%) were found in the tail region, with 38% on the dawn or dusk flank. For these cases there was no vortex activity near local noon, and very few for the duskside region (15%).

Vortices on the flanks for the southward cases were smaller in diameter and much more disordered than cases found with northward IMF. It was not clear which axis corresponded to their rotation axis, or whether their rotation was clockwise or counterclockwise. However, we found that most magnetotail vortices were more organized than on the flanks, and had the $z$-axis as their approximate rotation axis. In Figure 4.11 an example is shown of three vortices that formed in the magnetotail. The vortices rotate around the $z$-axis, but one rotates clockwise (upper), while the other two rotate counter-clockwise (bottom-right). No preference of rotation was seen in general for vortices in the magnetotail or those at the flanks for the southward cases.

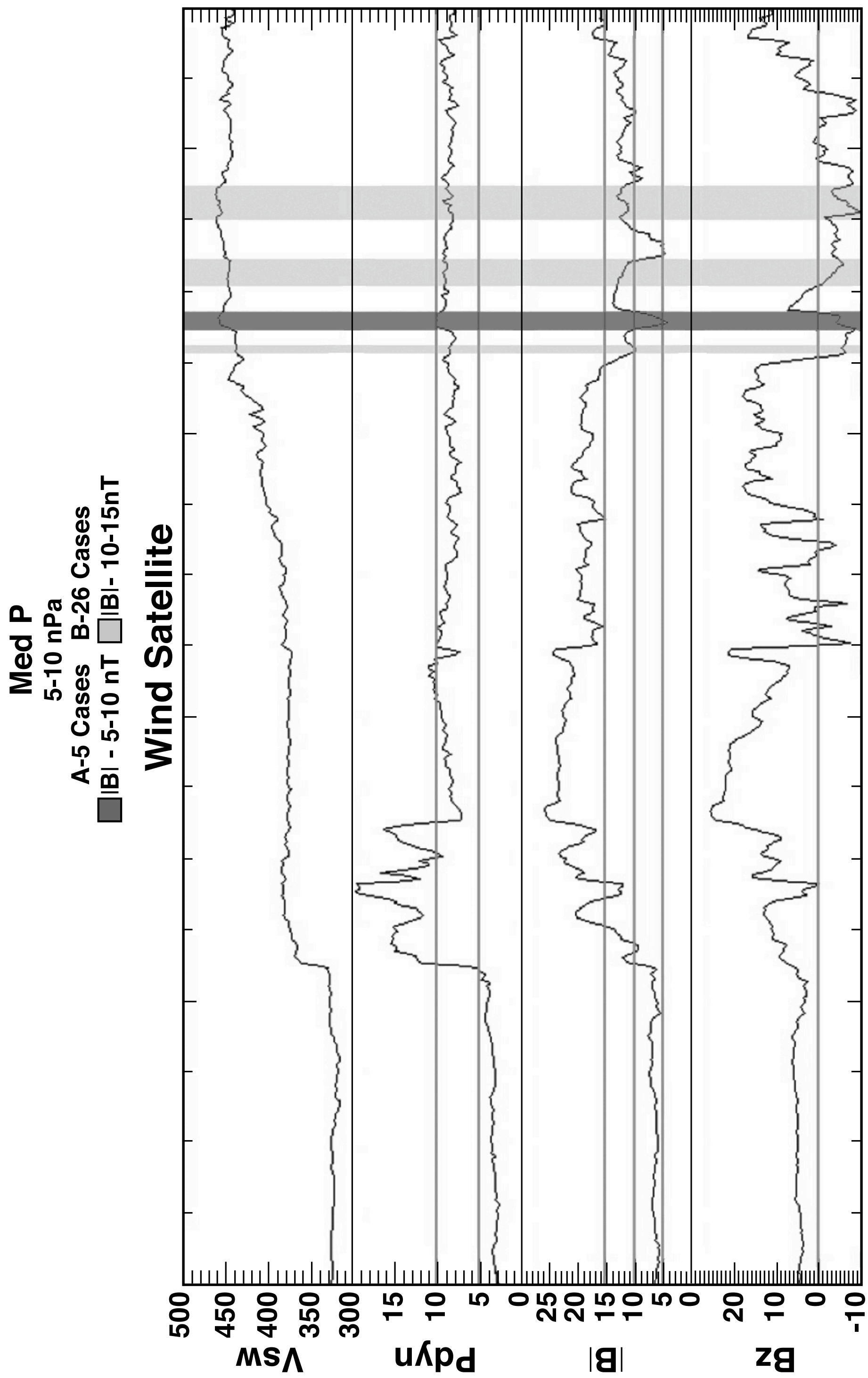


Figure 4.9: Vortices localized on the magnetopause for southward IMF. The colored regions show where vortices developed separated by two different magnetic field magnitude values, but only one dynamic pressure range.

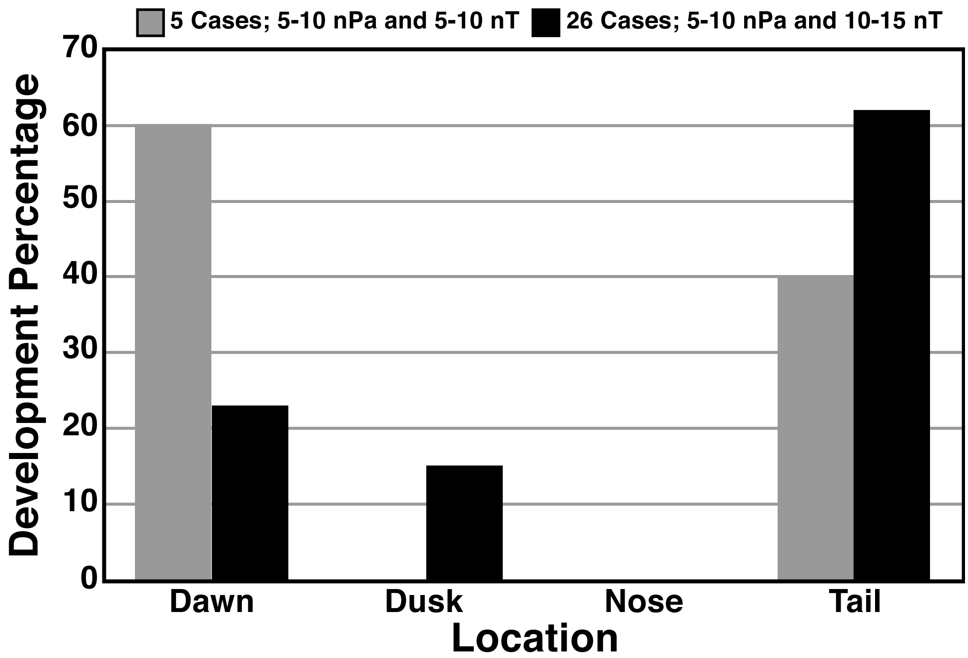


Figure 4.10: Percentages of vortices localized with southward IMF. When the magnetic field magnitude increased the vortices were most developed on the magnetotail than in any other location on the magnetosphere.

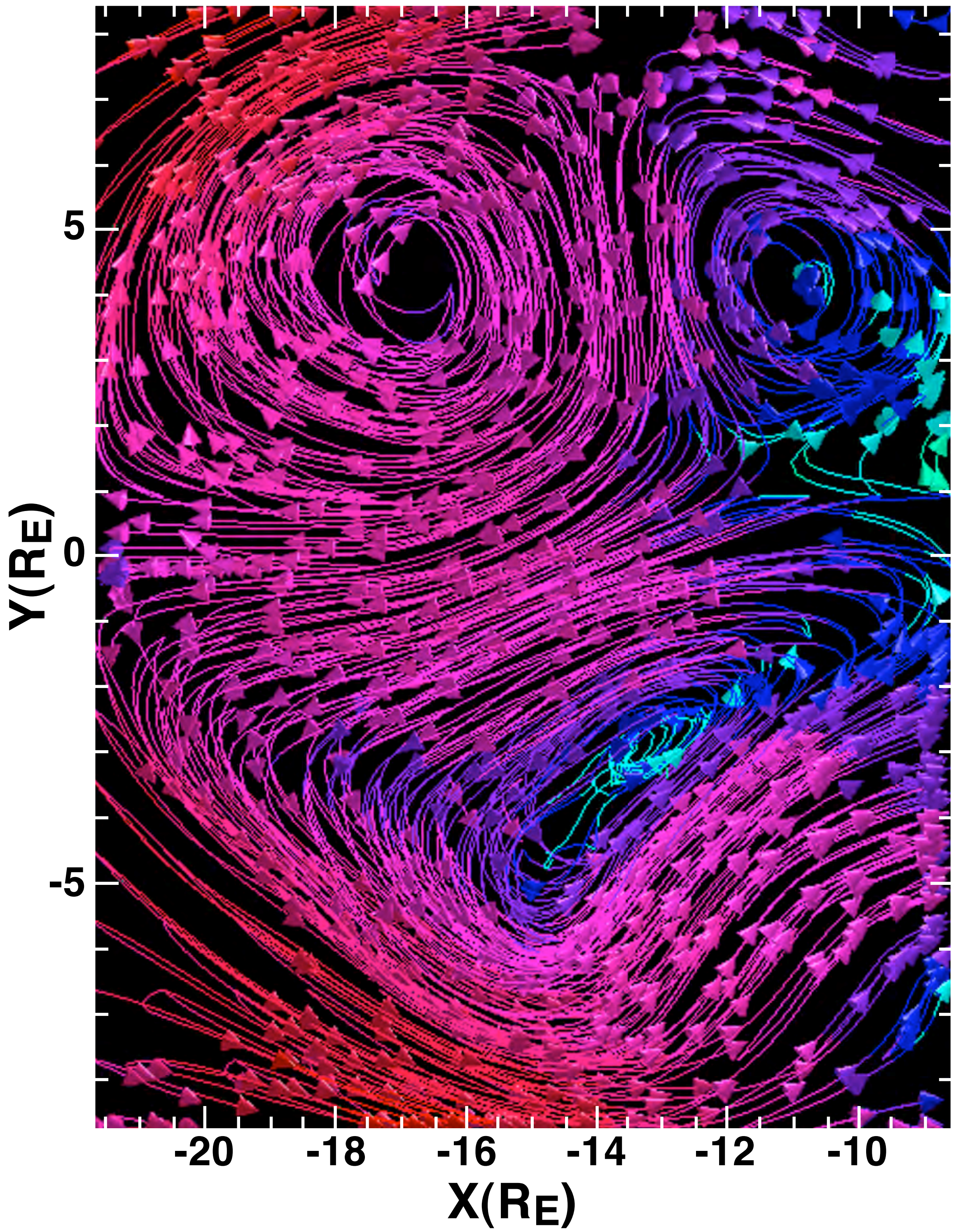


Figure 4.11: Three tail vortices formed under southward IMF. These vortices correspond to March 30 0419 UT.

# Chapter 5

# MHD simulation comparison with spacecraft observations

Magnetopause crossings observed by a spacecraft in the vicinity of the boundary can be analyzed for surface waves and vortical motion. For the high speed stream interval shown in Figure 3.2 the Geotail satellite is skimming along the magnetopause, well situated to observe boundary crossings. Figure 5.1 shows the orbit of Geotail in the *x*-*y* plane from March 29 2000 UT through April 2. At the beginning of the interval Geotail is located on the dawnside of the magnetosphere at a radial distance of 27 $R_E$ as highlighted in Figure 5.1. With the large solar wind pressure increase at 2215 UT on March 29 the magnetopause is compressed and Geotail is then near the dawn magnetopause boundary. The time interval from March 29 2000 to March 30 0500 UT, that corresponds to the MHD simulation interval, is marked with frequent magnetopause and boundary layer crossings by Geotail. We discuss below the properties of the physical parameters in the different regions encountered by boundary crossings, and we identify vortex-like conditions.

A data plot shown in Figure 5.2 with magnetic and plasma characteristics from the MGF and CPI instruments, allows us to follow the plasma behavior throughout the nine hours of the study. From top to bottom, the panels in Figure 5.2 show the magnetic field magnitude, the x and z com-

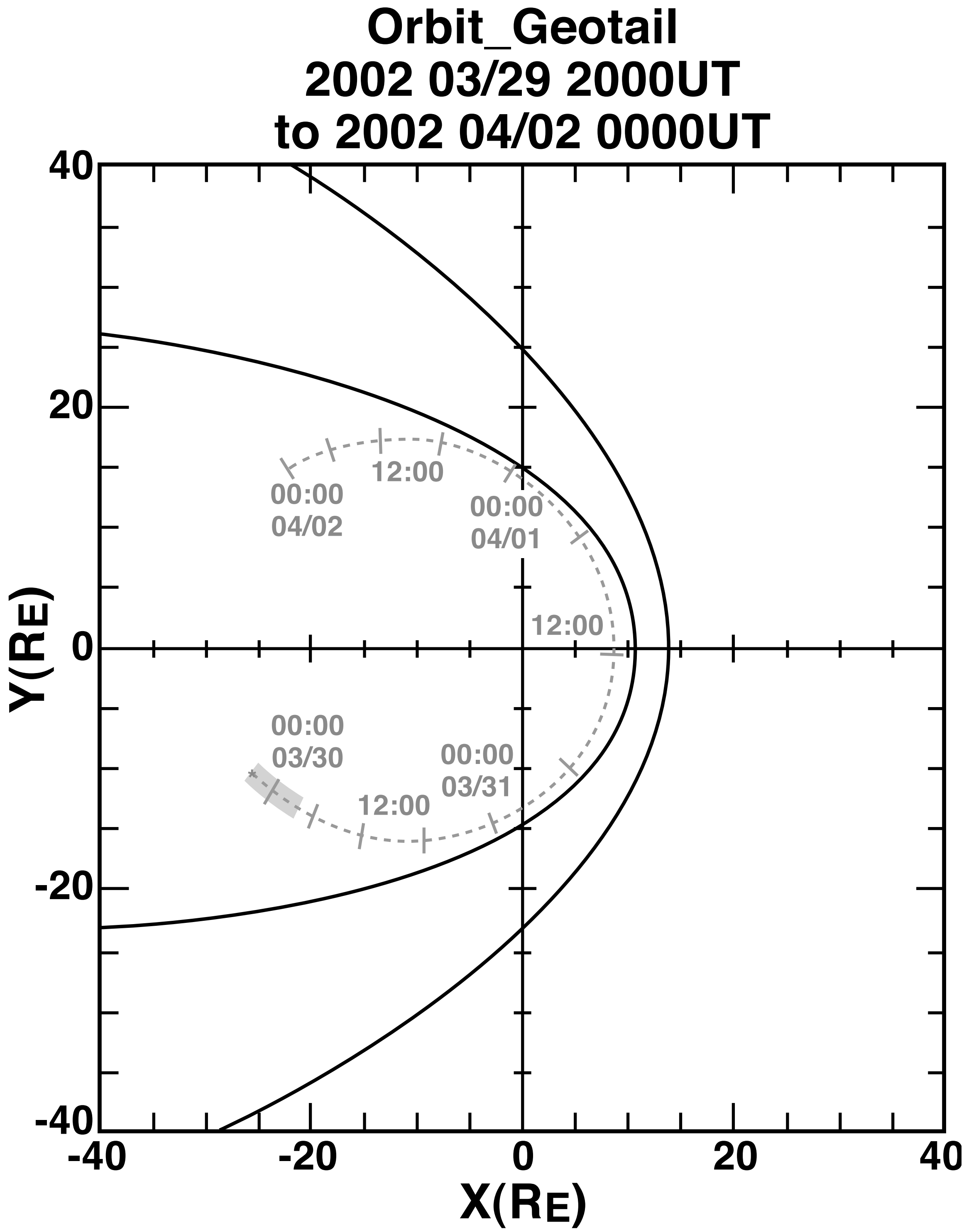


Figure 5.1: Geotail orbit of four and half days including the nine hours of the MHD simulation. The nine hours correspond to the colored region at the beginning of the orbit.

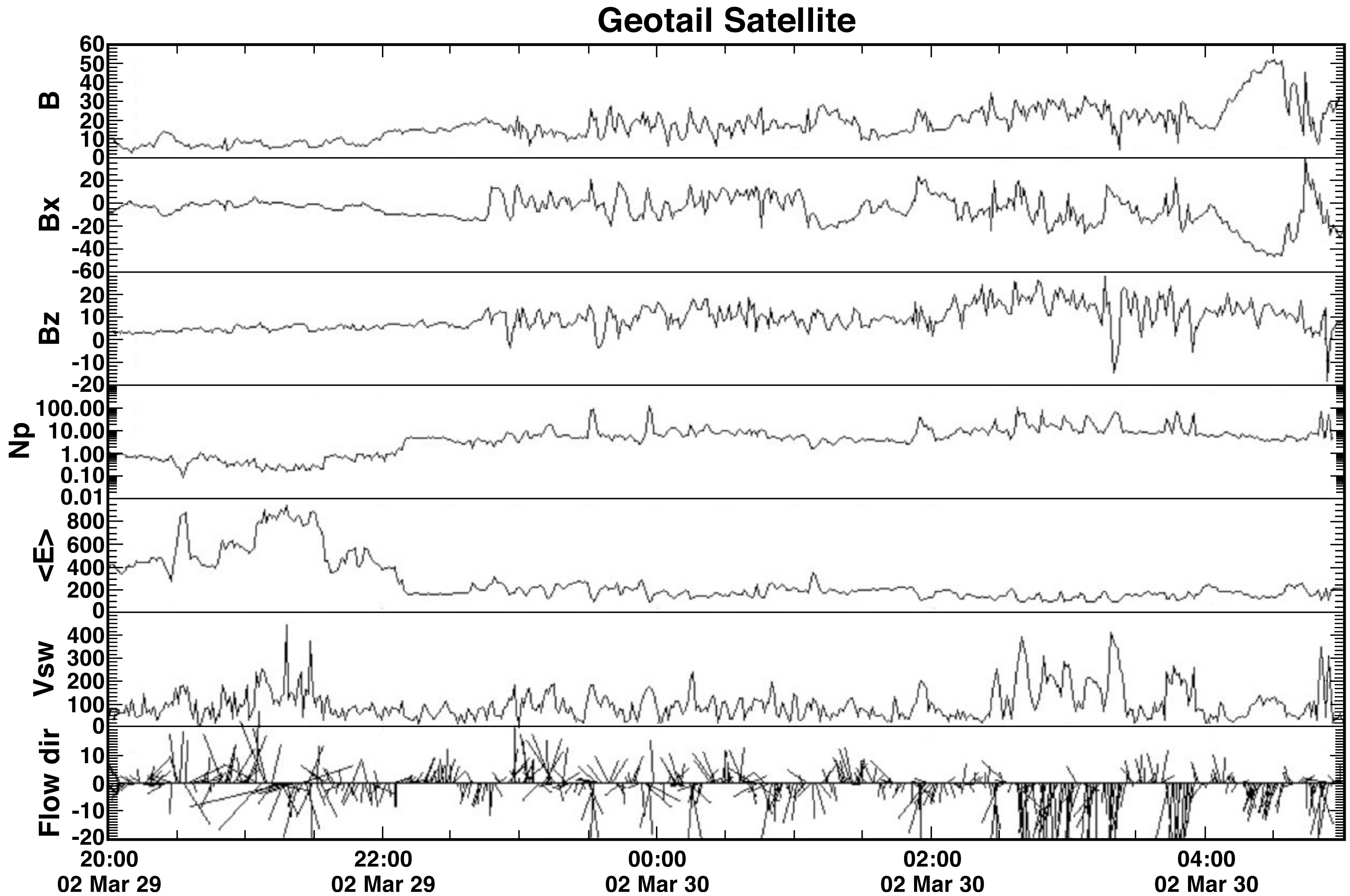


Figure 5.2: Nine hours of Geotail MGF and CPI data are plotted here corresponding to the last four hours of March 29 and the first five hours of March 30, 2002, which are the nine hours of the MHD simulation interval. Many boundary crossings can be seen beginning around 2200 UT.

ponents of the magnetic field, the ion density, average energy and flow speed. The last panel shows the plasma flow direction which is sunward (+*x*) direction if bars point up and in the antisunward (-*x*) direction if bars point down. The flow is also shown in the +(-)*y* direction if bars point right(left). For the first two hours no boundary crossings are seen. The magnetic field magnitude is very stable and the plasma has high average energy, low density and fluctuating velocity corresponding to conditions inside the magnetosphere in the plasma mantle. Particle counting statistics are low in this region so that the flow direction is volatile. Beginning around 2200 UT Geotail moves into the boundary layer; the density increases and the energy decreases to a value of 200 eV. As Geotail gets farther into the boundary layer the fluctuations in the magnetic field increase. Geotail stays in the boundary layer for an extended period of time with short excursions into the magnetosheath. In the magnetosheath region the particles have high density, high velocity, low energy and organized flow in the tailward direction. Two quick excursions into the magnetosheath are seen at about 2330 UT on March 29 and just before midnight on March 30. In the last two hours in Figure 5.2 many crossings can be seen from the boundary layer to the magnetosheath. These crossings correspond to short periods of time (1-10 minutes) that may be related to surface waves or compression and decompression of the magnetopause caused by solar wind pressure changes.

Figure 5.3 shows a higher resolution view of two hours in Figure 5.2, from 2300 on March 29 until 0100 on March 30. During this short interval Geotail is located on the dawnside of the magnetosphere at (-24, -12.38)$R_E$ in the *x*-*y* plane (SM coordinates), moving approximately 1 $R_E$ in the +*x*,-*y* direction every two hours. The plasma flow directions during these two hours rotate in a systematic way for minutes at a time that suggests Geotail may be passing through vortical flow. The decreases in speed to very low values may be due to Geotail being located near the center of a flow vortex. The higher speed flow may be near the outer regions of the flow vortex. To validate this supposition we show, in Figure 5.4, 2D snapshots in the *z*=0 plane from the MHD simulation for the time period of 2325-2333 UT highlighted in Figure 5.3. The panels in Figure 5.4 are successive time steps (1 min resolution) in the simulation; each stretches from -8 to -25

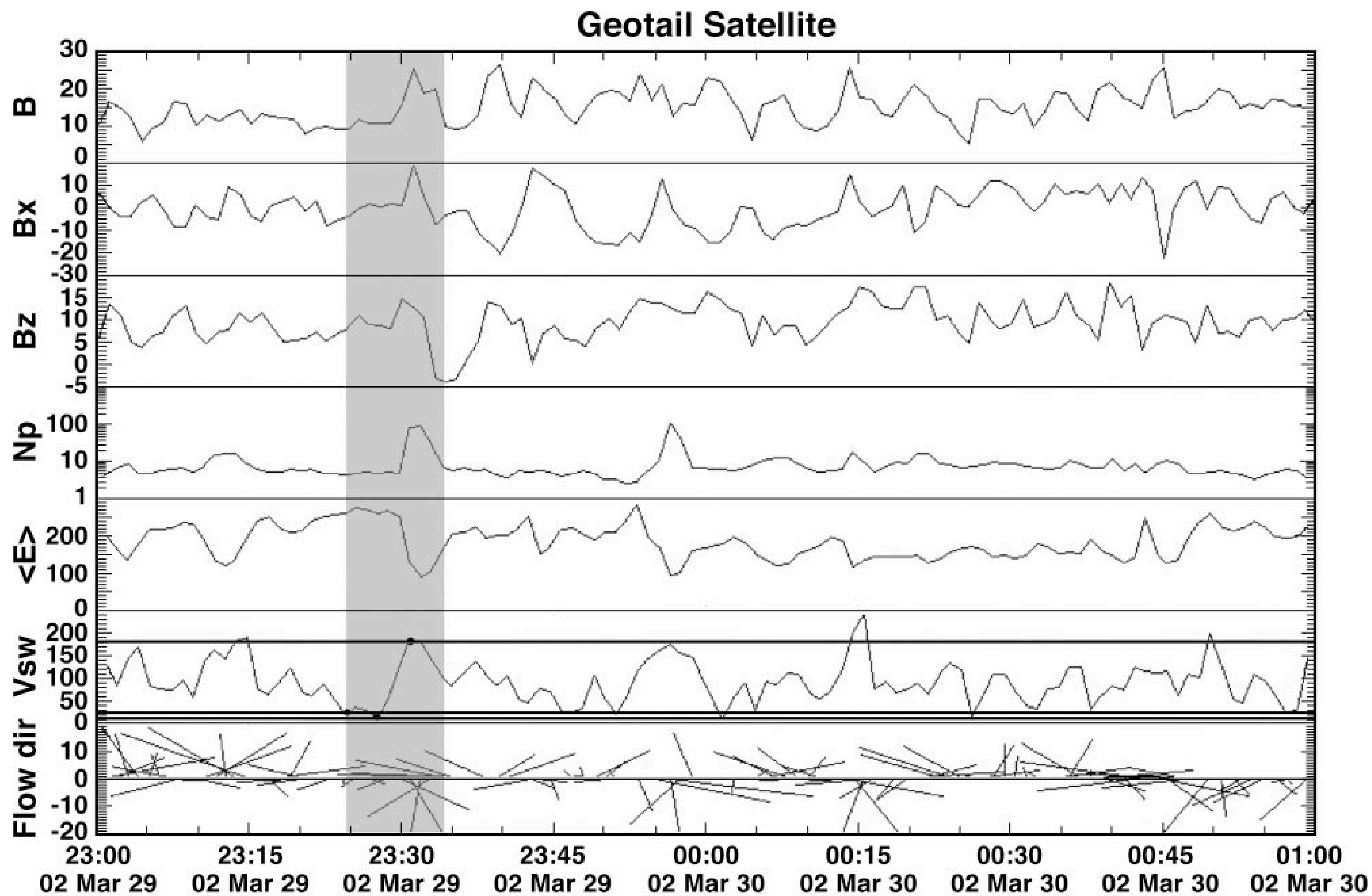


Figure 5.3: Two hours data plot from March 29 2300 UT to March 30 0100 UT. Comparisons were made between the highlighted time and the plasma velocity magnitude and flow direction in the simulation data.

$R_E$ in the *x*-direction and from -5 to -20 $R_E$ in the *y*-direction. Two separate vortices develop and are observed in the simulation panels, both move downstream (to the left in the -*x* direction) in successive time steps. The crossed lines in Figure 5.4 mark the approximate position of the Geotail satellite in the simulation; for these few minutes Geotail is essentially stationary and plasma flows past it. (We note that the *x* locations differ by about 10 $R_E$ between the Geotail data and simulation data. The *y* locations are nearly the same.)

Comparing observed plasma speeds and flow directions in Figure 5.3 to the MHD simulation snapshots shown in Figure 5.4, we can see many similarities. Observed flow direction vectors have been drawn on the simulation panels for easier comparison between simulation and data, however in some cases more than one vector has been drawn because the observed data is at 45 seconds resolution compared to one-minute resolution for the simulation. In the top left panel of Figure 5.4 the simulation flow speed at the approximate Geotail location marked by the crossed lines is about 20 km/s. This panel corresponds to 2325 UT in Figure 5.3 where the observed Geotail flow speed is 20 km/s. The flow directions are reasonably consistent between simulation and observation given the approximate location of Geotail. In the succeeding top panels of Figure 5.4 a vortex has developed and Geotail is near the center. The dark area around the vortex represents a value of 10 km/s; the simulation flow directions are highly variable near the vortex. These panels correspond to 2326-2327 UT in Figure 5.3 where the observed Geotail flow speeds are low, about 10 km/s and the flow directions are consistent with the simulation. In the middle left panel of Figure 5.4 Geotail remains in the vortex, but in the following two middle panels the vortex moves downstream (to the left) and Geotail is in faster flow. In the bottom panels a new vortex is visible but Geotail remains in the faster flow region 100-200 km/s. Geotail observes flow speeds up to 180 km/s during these last minutes in Figure 5.3. Geotail's observed flow direction rotates from largely +*y* (upward, antisunward) to -*x* (antisunward) to largely -*y* (downward, antisunward). These flow directions would be observed if Geotail passed through the outer regions of a somewhat larger vortex than that seen in the bottom three panels of Figure 5.4, as the vortex moved downtail.

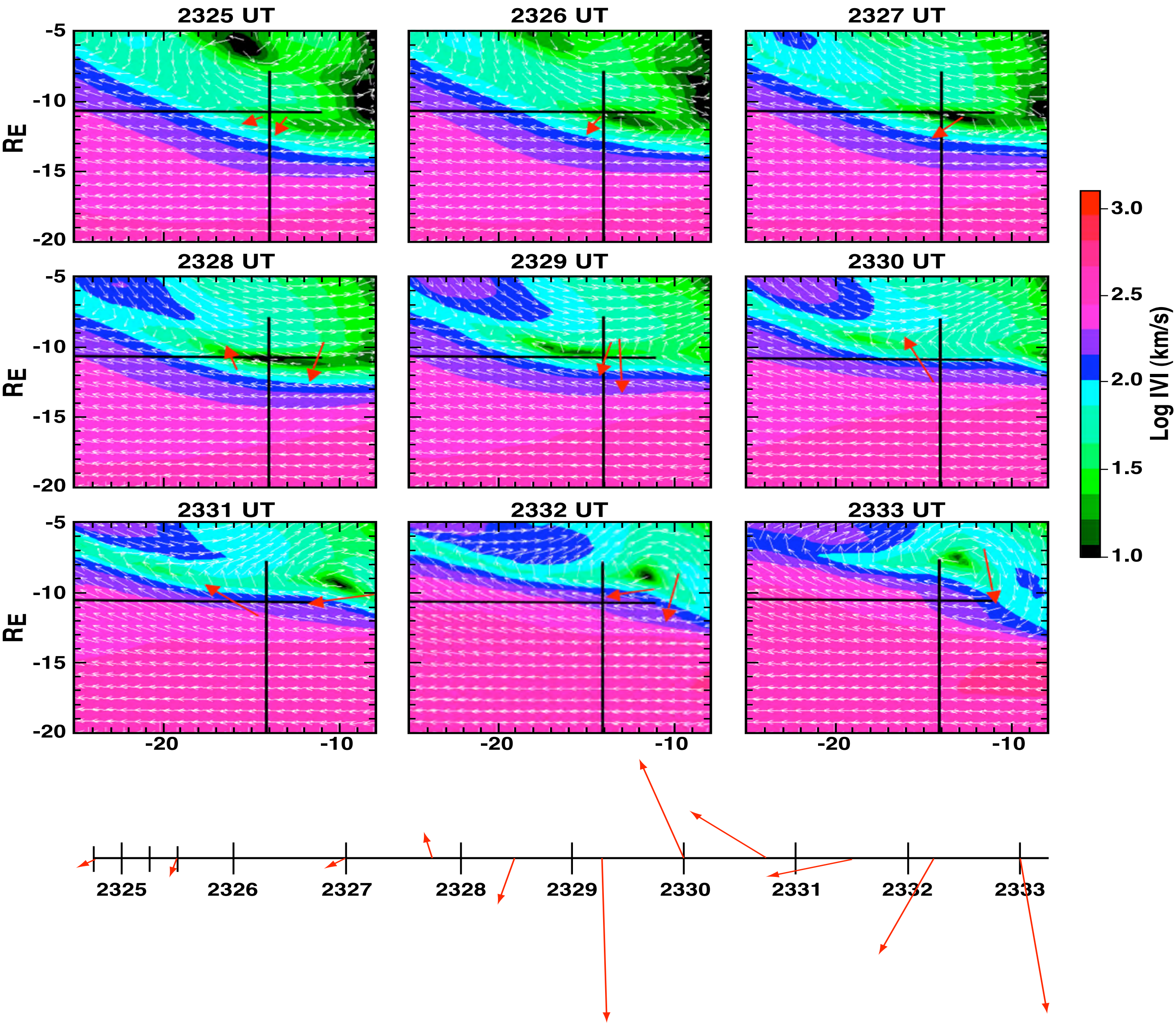


Figure 5.4: 2D Dawn flank snapshots for March 29 2325-2333 UT with Geotail's location marked at approximate -14,-10.5 $(x,y)$RE. Velocity changes can be seen for the data interval shown in Figure 5.3. Plasma flow direction vectors that correspond to the actual spacecraft data shown in Figure 5.3 were also drawn for better comparison.

Geotail observations in Figure 5.3 show alternating times of high and low speed and with some other systematic rotations in flow direction that are in keeping with vortical flow as discussed above. The repeating pattern could be different vortices propagating downtail that pass by the Geotail satellite. Higher time and spatial resolution MHD simulations and higher resolution observations should improve the comparisons.

# Chapter 6

# Conclusions

Since 1960, the study of solar wind effects on Earth's magnetosphere has played an important role in space physics. A KH instability near the magnetopause is one of the processes driven by the solar wind that could contribute significantly to the transport of energy, momentum, and mass into the Earth's magnetosphere. Many theoretical models and simulations have been developed to study this instability. In our study a combination of MHD simulation and an IDL visualization tool were used to search for vortices in the magnetosphere during a time when upstream Wind observations showed a high speed solar wind stream. In total we found 273 vortices near the magnetopause during northward IMF, and 31 vortices with southward IMF.

The vortices that developed under northward IMF conditions were large scale in diameter (up to 10 RE), and also were more prevalent on the dawnside than on the duskside. Those on the dawnside were less ordered and had a preference to rotate in the clockwise direction. On the other hand, those on the duskside were more ordered and tended to rotate counter-clockwise. These preferences in rotation, clockwise for dawnside vortices and counter-clockwise for duskside vortices, can be described by the polarization of surface waves that could be driven by KH instability near the magnetopause. The polarity of observed vortices changes approximately near noon where the plasma flow divides to flow around the magnetopause. Waves in the morning (dawn) travel

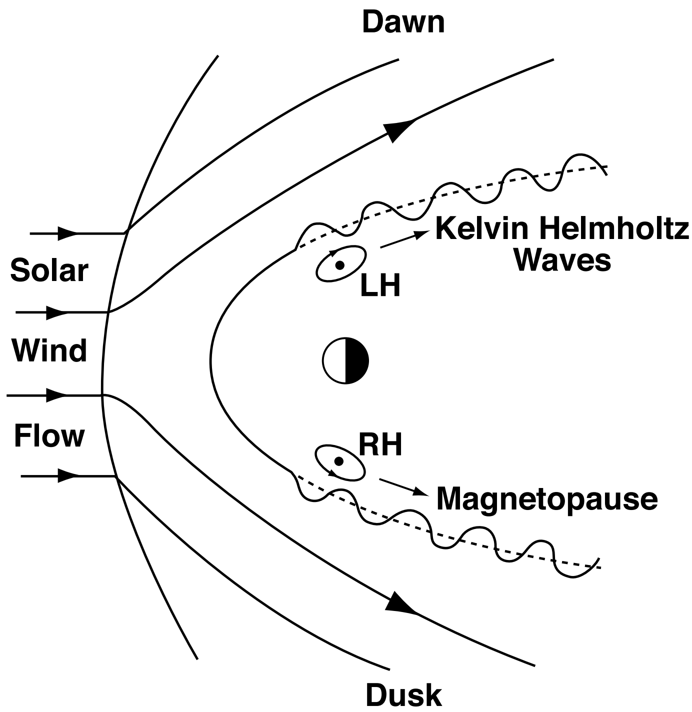


Figure 6.1: From Hughes [1994]. Polarization change of surface waves driven by a KH instability. Waves in the morning travel westward and those in the evening travel eastward.

westward (clockwise) and those in the evening (dusk) travel eastward (counter-clockwise). The polarization change can be seen in Figure 6.1 from Hughes [1994]. This kind of behavior has also been seen in other studies. For example, Hones et al., [1978] found that vortex rotations in the morning and evening sectors were clockwise when viewed from above the ecliptic plane in the morning sector and counter-clockwise on the evening sector.

We also found that the dawnside could have more than one vortex at the same time, at least one of them rotated clockwise. The disorder and number of vortices on the dawnside are most likely the result of being downstream from the turbulent quasi-parallel bow shock that forms on the dawnside [e.g. Tsurutani et al., 1981]. Some substantial vortex activity was also found near local noon time showing that waves can begin to grow close the subsolar point where the flow is very slow [Spreiter and Alksne, 1969]. Their cause is still not evident, specially when talking about KH instability.

On the contrary, vortices that develop with a southward IMF were less ordered on the flanks. Their rotation axis and their rotation direction were not clearly distinguished. Also, when the magnetic field magnitude and the dynamic pressure began to increase, comparatively more vortices developed in the tail region of the magnetosphere compared to what was observed for vortices associated with northward IMF. It was not possible to determine a preference of rotation for these tail vortices, not even for the ones that developed on the boundary flanks. Also, at this time less vortex development was found, which may be attributed to the increase in pressure. The pressure changes could perturb the magnetopause, compressing and decompressing the magnetosphere [e.g., Sibeck et al., 1989].

Boundary crossings seen by the Geotail spacecraft were also studied for the nine-hour time interval. A comparison of plasma flow velocities and directions observed with actual spacecraft data was made to validate our results from the MHD simulation. These observations are similar to the ones showed by Fairfield et al. [2000]. We showed plasma flow directions rotating in a systematic way for minutes at a time that suggest Geotail may be passing through vortical flow. The low flow speeds observed by Geotail could be near the center of a flow vortex, and the higher flow speeds could be observed near the outer regions. Flow vortices in MHD data in the vicinity of Geotail and the satellite observing systematically rotating flow suggest a strong likelihood of the existence of flow vortices near the magnetopause flanks.

The magnetosphere's reaction to different solar wind conditions during our study and associated vortex development suggest the presence of a KH instability near the magnetopause boundary. However, the majority of vortices with northward IMF (47%) occurred before the onset of the high speed stream, and also before increases in dynamic pressure and magnetic field magnitude. The only condition in our data that could systematically contribute to a KH instability at this time is the northward IMF. However, as seen in Figure 3.2, there is a magnetic field component in the ecliptic plane to stabilize the KH instability. For all the other cases, the northward IMF, the consistent high speed stream, vortex evolution and rotation preference are all consistent with a KH instability.

Large scale vortices driven by a KH instability could play an important role in carrying energy and particles into the magnetosphere. Our MHD visualization tool is highly effective for understanding the development of vortices near the outer magnetospheric boundary, the conditions at which they evolve, and the required parameters needed for this instability to take place at the magnetopause. A manuscript with these results was submitted and accepted for publication at the Journal of Geophysical Research (JGR) - Space Physics in December 2006. A later paper will discuss the changes in particle density and energy flux within the flow vortices and between the manetosheath and magnetosphere. We will also examine more cases of vortex development in MHD simulation data driven by systematically changing solar wind conditions. The volume of data in this study demands an automated approach. Work is being done to implement new vortex identification algorithms in the visualization tool to permit an automated and faster detection method for vortices within the time series of the simulation data.

# Bibliography


[1] Bargatze, L. F., D. N. Baker, R. L. McPherron, and E. W. Hones, Jr., Magnetospheric Impulse Response for Many Levels of Geomagnetic Activity, *J. Geophys. Res., 90*, 6387, 1985.

[2] Chen, S. -H., M. G. Kivelson, On nonsinusoidal waves at the Earth's magnetopause, *Geophys. Res. Lett., 20*, 2699, 1993.

[3] Chen, S. -H., M. G. Kivelson, et al., Anomalous aspects of magnetosheath flow and of the shape and oscillations of the magnetopause during an interval of strongly northward interplanetary magnetic field, *J. Geophy. Res., 98*, 5727, 1993.

[4] Collado-Vega, Y. M., R. Kessel, X. Shao, R. Boller, MHD flow visualization of magnetopause boundary region vortices observed during high speed streams, *J. Geophys. Res.*, 2006 (in press).

[5] Enseeiht, Kelvin-Helmholtz Instability. http://www.enseeiht.fr/hmf/travaux/CD0001/travaux /optmfn/hi/01pa/hyb72/kh/kh_theo.htm.

[6] Dungey, J. W., Interplanetary magnetic fields and the auroral zones, *Phys. Rev. Lett., 6*, 47, 1961.

[7] Fairfield, D. H., A. Otto, et al., Geotail observations of the Kelvin-Helmholtz instability at the equatorial magnetotail boundary for parallel northward fields, *J. Geophys. Res., 105*, A9, 21159, 2000.

[8] Fedder, J. A., J. G. Lyon, S. P. Slinker, and C. M. Mobbary, Topological structure of the magnetotail as function of interplanetary magnetic field and with magnetic shear, *J. Geophys. Res., 100*, 3613, 1995.

[9] Frank, L. A., et al., Comprehensive Plasma Instrument (CPI), In Geotail Prelaunch Report, SES-TD-92-007SY, Institute of Space and Astronautical Science, SES Data Center, 179-238, 1992.

[10] Fujimoto, M., T. Terasawa, Anomalous ion mixing within an MHD scale Kelvin-Helmholtz vortex, *J. Geophys. Res., 99*, A5, 8601, 1994.

[11] Guzdar, P. N., X. Shao, M. Wiltberger, C. C. Goodrich, K. Papadopoulos, J. G. Lyon, Three-dimensional MHD simulations of the steady-state magnetosphere with northward interplanetary magnetic field, *J. Geophy. Res., 106*, 275, 2001.

[12] Hasegawa, A., *Plasma instabilities and non-linear effects, Chap. 3*, Springer-Verlag, New York, 1975.

[13] Hasegawa, H., M. Fujimoto, K. Takagi, et al., Single-spacecraft detection of rolled-up Kelvin-Helmholtz vortices at the flank magnetopause, *J. Geophys. Res., 111* A09203, doi:10.1029/2006JA011728, 2006.

[14] Hones, E. W., Jr., G. Paschmann, et al., Vortices in magnetospheric plasma flow, *Geophys. Res. Lett., 5*, 2069, 1978.

[15] Hughes, W. J., Magnetospheric ULF Waves: A tutorial with a historical perspective, *Geophysical Monograph, 81*, 1, 1994.

[16] Kivelson, M. G., S. -H. Chen, The Magnetopause: Surface waves and instabilities and their possible dynamical consequences, in *Physics of the Magnetopause, Geophys. Monogr. Ser.*,

vol. 90, edited by P. Song, B. U. O. Sonnerup, and M. F. Thomsen, pp. 257,-268, AGU, Washington, D. C., 1995.

[17] Kokubun, S., T. Yamamoto, et al., The GEOTAIL magnetic field experiment, *J. Geomag. Geoelectr., 46*, 7-21, 1994.

[18] Lepping, R. P., M. H. Acuna, et al., The Wind Magnetic Field Investigation, in The Global Geospace Mission, ed. C.T. Russell, Kluwer Academic Pub., 207-229, 1995.

[19] Lyon, J. G., J. A. Fedder, and C. M. Mobarry, The Lyon-Fedder-Mobarry (LMF) Global MHD Magnetospheric Simulation Code, *J. Atm. And Solar-Terrestrial Phys., 66*, Issue 15-16, 13333-1350, 2004.

[20] Miura, A., Anomalous Transport by Magnetohydrodynamic Kelvin-Helmholtz instabilities in the Solar Wind-Magnetosphere Interaction, *J. Geophys. Res., 89*, A2, 801, 1984.

[21] Miura, A., Simulation of Kelvin-Helmholtz instability at the magnetospheric boundary, *J. Geophys. Res., 92*, A4, 3195, 1987.

[22] Miura, A., Kelvin-Helmholtz instability at the magnetospheric boundary: dependence on the magnetosheath sonic Mach number, *J. Geophys. Res., 97*, A7, 10655, 1992.

[23] Miura, A., Dependance of the magnetopause Kelvin-Helmholtz instability on the orientation of the magnetosheath magnetic field, *Geophys. Res. Lett., Vol. 22*, No. 21 , 2993, 1995.

[24] Ogilvie, K. W., R. J. Fitzenreiter, The Kelvin-Helmholtz instability at the magnetopause and inner boundary layer surface, *J. Geophys. Res., 94*, A11, 15113, 1989.

[25] Ogilvie, K.W., D. J. Chornay, et al., SWE, Comprehensive Plasma Instrument for Wind Spacecraft, in Global Geospace Mission, ed. C.T. Russell, Kluwer Academic Pub., 55, 1995.

[26] Otto, A., D. H. Fairfield, Kelvin-Helmholtz instability at the magnetotail boundary: MHD simulation and comparison with Geotail observations, *J. Geophys. Res., 105*, A9, 21175, 2000.

[27] Papadopoulos, K., C. Goodrich, M. Wiltberger, R. Lopez, and J.G. Lyon, The Physics of Substorms as revealed by ISTP, *Phys. Chem. Earth(C), Vol. 24*, No. 1-3, 189-202, 1999.

[28] Papadopoulos, K., The role and form of modeling in space physics, *Phys. Chem. Earth(C), Vol. 25*, No. 1-3, 2000.

[29] Parks, G.P., *Physics of Space Plasmas An Introduction*, Westview Press, 2004.

[30] Ronnmark, K., Space Physics, Department of Physics, UmeåUniversity. http://www.tp.umu.se/forskning/space/.

[31] Shao, X. ; P. N. Guzdar, K. Papadopoulos, C.C. Goodrich, A.S. Sharma, G.M. Milikh, M.J. Wiltberger, J.G. Lyon, Three-dimensional MHD simulations of the Earth's magnetosphere on Feb 9-10 1995 for northward interplanetary magnetic field and comparison of the lobe field with Geotail observations, *Geophys. Res. Lett., Vol. 28*, No. 20 , 3835, 2001.

[32] Shao, X., M. I. Sitnov, S.A. Sharma, K. Papadopoulos, C.C. Goodrich, P.N. Guzdar, G.M. Milikh, M.J. Wiltberger, and J.G. Lyon, Phase transition-like behavior of magnetospheric substorms: Global MHD simulation results, *J. Geophys. Res., 108* (A1), doi:10.1029/2001JA009237, 2003.

[33] Sibeck, D. G., W. Baumjohann, R.C. Elphic, D.H. Fairfield, et al., The magnetospheric response to 8-minute period strong-amplitude upstream pressure variations, *J. Geophys. Res., 94*, 2505, 1989.

[34] Spreiter, J. R., A. Y. Alksne, Plasma flow around the magnetosphere, *Rev. Geophys., 7*, 11, 1969.

[35] Takagi, K., C. Hashimoto, H. Hasegawa, et al., Kelvin-Helmholtz instability in a magnetotail flank-like geometry: Three dimensional MHD simulations, *J. Geophys. Res., 111* A08202, doi:10.1029/2006JA011631, 2006.

[36] Tsurutani, B. T., P. Rodriguez, Upstream waves and particles: an overview of ISEE results, *J. Geophys. Res., 86*, No. A6, 4319, 1981.

[37] Wei, C. Q., L. C. Lee, A. L. La Belle-Hamer, A simulation study of the vortex structure in the low-latitude boundary layer, *J. Geophys. Res., 95*, A12, 20793, 1990.

[38] Wiltberger, M., T. I. Pulkkinen, J. G. Lyon, and C. C. Goodrich, MHD simulation of the magnetotail during the December 10, 1997, substorm, *J. Goephys. Res., 105*, 27649, 2000.

# Appendix 1: Kelvin-Helmholtz Dispersion Relation

The Kelvin-Helmholtz instability arises when waves are excited at boundaries with velocity shears. The non-linear stage of this instability can create vortex events that can lead to the interaction between the fluids of the two sides of the boundary. Considering a boundary with a velocity shear, the dispersion relation for KH waves can be written as

$$
\begin{aligned}
w' = \frac{\rho_1 \mathbf{U}_1 \cdot \mathbf{k} + \rho_2 \mathbf{U}_2 \cdot \mathbf{k}}{(\rho_1 + \rho_2)} \pm \frac{1}{(\rho_1 + \rho_2)} \{(\rho_1 + \rho_2)[\rho_1 (\mathbf{V}_{A1} \cdot \mathbf{k})^2 + \\
\rho_2 (\mathbf{V}_{A2} \cdot \mathbf{k})^2] - \rho_1 \rho_2 (\Delta \mathbf{U} \cdot \mathbf{k})^2\}^{1/2}.
\end{aligned}
\tag{6.1}
$$

assuming that plasmas on the two sides of the boundary can be adequately approximated as MHD "fluids" and that these "fluids" are ideal, incompressible and with a isotropic pressure. Here $w'$ is the Doppler-shifted frequency measured by an observer stationary on the boundary, $\rho$ is the fluid density, **U** the fluid velocity, and **k** the wave propagation vector. The subscripts *1* and *2* refer to each side of the boundary. It has also been applied

$$
\mathbf{V}_{A1} = \mathbf{B}_1 \cdot \mathrm{k}/(\mu_0 \rho_1)^{1/2} \text{ and } \mathbf{V}_{A2} = \mathbf{B}_2 \cdot \mathrm{k}/(\mu_0 \rho_2)^{1/2} \tag{6.2}
$$

where **B** is the magnetic field, and $\mathbf{V}_\mathrm{A}$ is the Alfvén velocity. The first term in equation (6.1) represents the effects of density between the two sides, the second term implies the effect of the magnetic field on the fluids movement and the third term represents the disontinuites by the difference in velocity between the two sides of the boundary. The KH waves are unstable when the frequency, $w'$, is imaginary. Because **U, B,** and **k** all lie in the *x*-*y* plane this happens when

$$\rho_1\rho_2(\Delta\mathbf{U}\cdot\mathbf{k})^2 > \frac{1}{\mu_0}(\rho_1+\rho_2)[(\mathbf{B}_1\cdot\mathbf{k})^2+(\mathbf{B}_2\cdot\mathbf{k})^2 \tag{6.3}$$

To produce an instability, the velocity shear has to overcome the magnetic tension which will resist any force trying to stretch it. The nonlinear stage of this instability creates vortex events for which the growth rate depends on the **B, k**, and $\Delta\mathbf{U}$ relative direction. If $\mathbf{B}_1$ and $\mathbf{B}_2$ are perpendicular to **k**, then the right-hand side vanishes and $(\Delta\mathbf{U}{\cdot}\mathbf{k})^2 > 0$, which implies that the boundary is unstable to an arbitrarily small shear across the boundary [Parks, 2004].

# Appendix 2: Instrument Descriptions

Wind and Geotail spacecrafts constitute part of a cooperative satellite project in conjunction with Polar, SOHO and Cluster projects designated the International Solar Terrestrial Physics (ISTP) program. The objective of this program is to gain a better understanding of the physics behind the solar terrestrial relations.

The purpose of the Wind spacecraft is to measure the incoming solar wind, magnetic fields and particles. It has a cylindrical form with approximately 2.8 m in diameter by 1.25 m high, with body mounted solar cells. The long wire spin-plane antennas, inertial booms, and spin-plane appendages support the sensors on board. It has experiment booms deployed along both Z axes with a spin rate of 20 rpm around an axis within 1 degree of normal to the ecliptic. Wind is actually located sunward to the Sun-Earth gravitational equilibrium point (L1) with a variation of 235 to 265 Earth Radii.

The Wind spacecraft diagram is shown in Figure 6.2. We used the Magnetic Field Investigation (MFI) [Lepping et al., 1995] and Solar Wind Experiment (SWE) [Ogilvie et al., 1995] instruments from the Wind satellite. The MFI consists of a triaxial fluxgate magnetometer mounted remote from the spacecraft on a boom, a multiple resolution A/D converter, and a microprocessor-controlled range control logic and data processing system. Seven measurement ranges are included: plus or minus 16, 64, 256, 1024, 4096, 16,384, and 65,536 nT. Resolution ranges from 0.004 to 16 nT in normal mode and 2.5E-4 to 1 nT in high resolution mode. The objective of this instrument is to capture the fluctuations of the Interplanetary Magnetic Field (IMF) as a function of time to understand its complexity and observe how observed changes can be described by the dynamics changes of the magnetosphere.

The SWE instrument is a six-axis ion-electron spectrometer which provides three-dimensional velocity distribution functions for ions and electrons, with high time resolution. The energy range covered extends from 7 eV to 30 keV for electrons in four different modes, and from 30 eV to 30 keV in four different ion modes. In addition, two Faraday cups are used to obtain three-dimensional measurements of ions in 15-s periods, in the energy range 5 eV to 5 keV. This instrument is intended to provide an accurate measurement of the solar wind parameters in real time.

The Geotail spacecraft is intended to measure the energy flow of the magnetotail region to understand the physics of the magnetopause magnetospheric boundary regions, the plasma sheet, and reconnection and neutral line formation. The spin rate of the spacecraft is 20 rpm around a spin axis maintained between 85-89 degrees to the ecliptic plane. Geotail is cylindrical, 2.2 m in diameter, and 1.6 m high with body-mounted solar cells. Geotail has a back-up battery subsystem which operates when the spacecraft is in the Earth's shadow (limited to 2 hrs). Real-time telemetry data transmitted in X-band are received at the Usuda Deep Space Center (UDSC) in Japan. There are two tape recorders on board, each with a capacity of 450 Mb, which allows daily 24-hour data coverage and are collected in playback mode by the NASA Deep Space Network (DSN). It is actually located within its near-Earth orbit with an apogee varying from 50 $R_E$ to 30 $R_E$.

The Geotail diagram is shown in Figure 6.3. We used the Magnetic Field Measurement (MGF) [Kokubun et al., 1994] and Comprehensive Plasma (CPI) [Frank et al., 1992] instruments from the Geotail spacecraft. The MGF instrument consists of dual three-axis fluxgate magnetometers and a three-axis search coil magnetometer. Triad fluxgate sensors, which utilize a ring core geometry, are installed at the end and middle of a 6 m deployable mast. Three search coils are mounted approximately one-half of the way out on another 6 m boom together with search coils for the VLF wave in the PWI system. The fluxgate magnetometers are of standard design and consist of an amplifier, filter, phase sensitive detector, integrator, and a voltage-current convertor. The

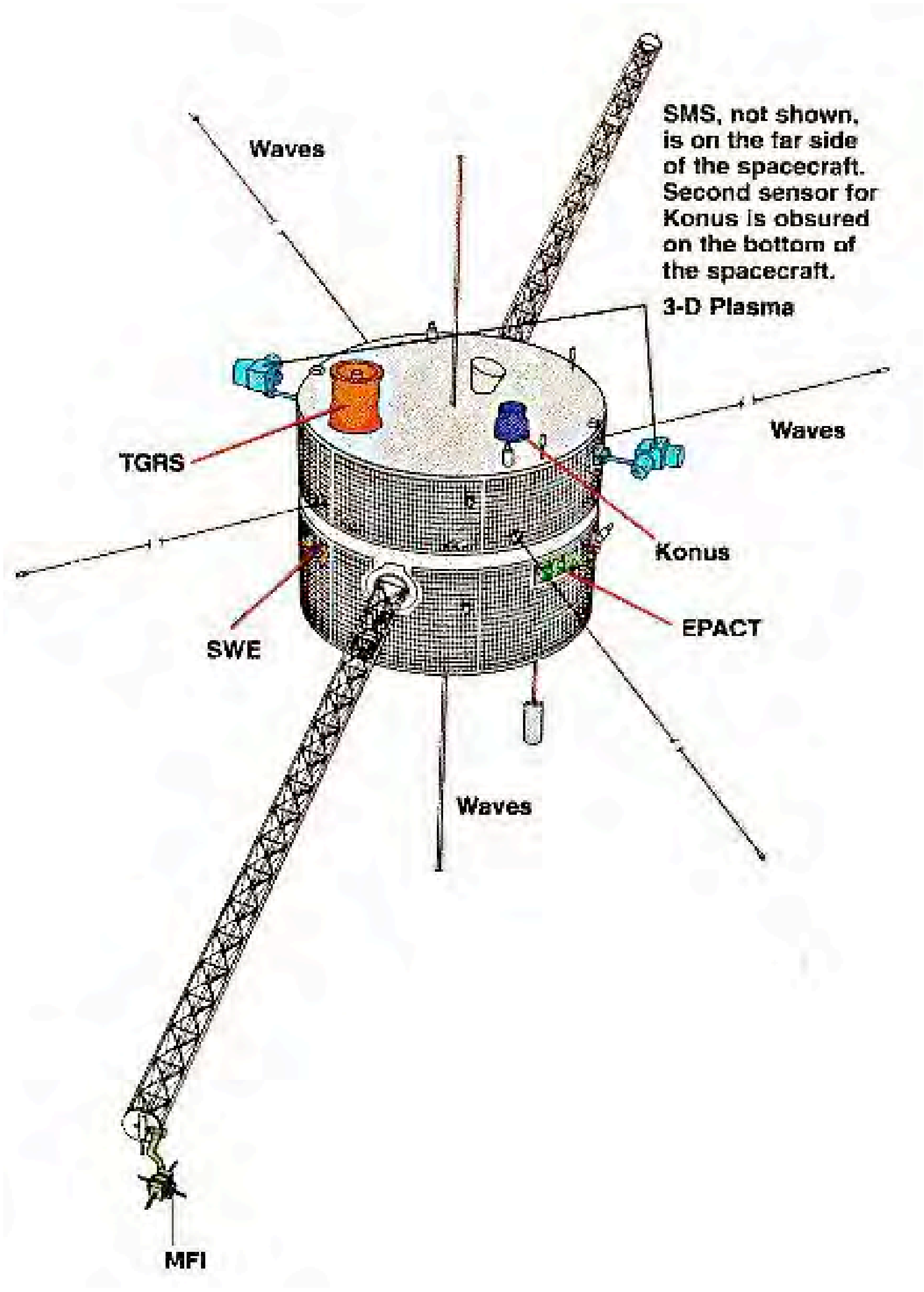


Figure 6.2: Wind diagram with all the instruments on board.

fluxgate magnetometers operate in seven dynamic ranges to cover various regions of the Earth's magnetosphere and the solar wind: +/-16 nT, +/-64 nT, +/-256 nT, +/-1024 nT, +/-4096 nT, +/-16384 nT, and +/-65536 nT, and supply 16 vectors/sec. The search coil magnetometer system consists of three sensors, preamplifier, amplifier, filter, multiplexer, and an A/D converter. The search coil magnetometers operate in a frequency range of 0.5 kHz to 1 kHz, and supply 128 vectors/sec. The fluxgate magnetometer operates in both real time and record modes, while the search coil data are used only in real time mode. The objective is to measure the magnetic field variation in the magnetotail between frequencies below 50Hz.

The CPI instrument contains three sets of quadrispherical analyzers with channel electron multipliers. These three obtain three-dimensional measurements for hot plasma and solar wind electrons, for solar wind ions, and for positive-ion composition measurements. The positive-ion composition measurement includes five miniature imaging mass spectrometers at the exit aperture of the analyzer, and covers masses from 1 to 550 u/Q at 100 eV, and 1 to 55 u/Q at 10 keV. The hot plasma analyzer measures electrons and ions in the range 1-50,000 eV/Q. The solar wind analyzer measures ions from 150 to 7,000 eV/Q. Sequencing of the energy analyzers and mass spectrometers, and other control functions, are provided by two microprocessors. Its objective is to observe three dimensional velocity distribution functions of positive ions and electrons, but making identification of ion species.

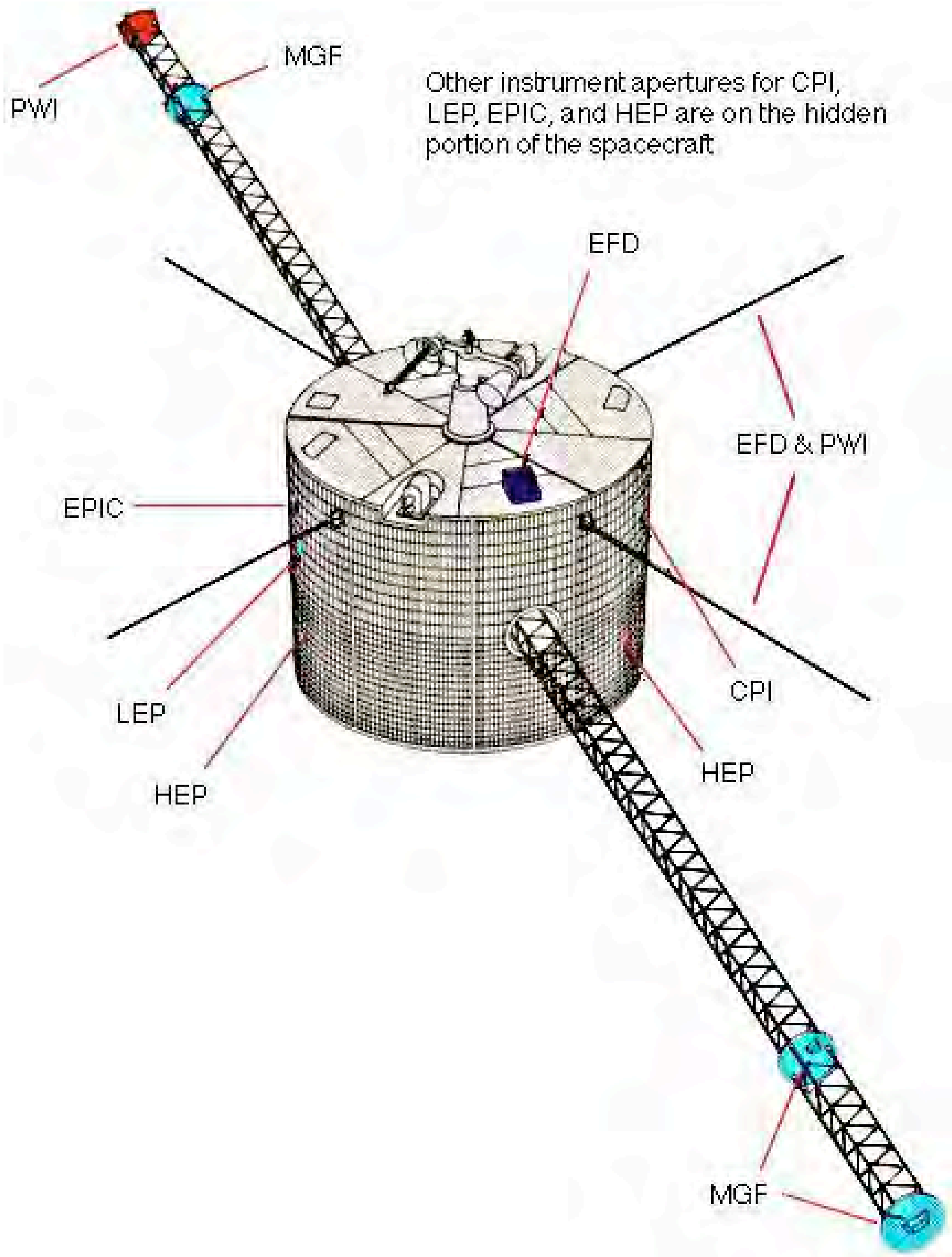


Figure 6.3: Geotail diagram with all the instruments on board.